Inorg. Chem. **2008**, *47*, 4861−4876

Synthesis, Structure, and Physical Properties of a New Anions-Controlled Cd(II)-Guanazole (3,5-Diamino-1,2,4-triazole) Hybrid Family

Rui-Bo Zhang,[†,‡] Zhao-Ji Li,[†] Ye-Yan Qin,[†] Jian-Kai Cheng,[†] Jian Zhang,[†] and Yuan-Gen Yao*[,†]

The State Key Laboratory of Structural Chemistry, Fujian Institute of Research on the Structure of Matter, The Chinese Academy of Sciences, Fuzhou, Fujian 350002, P.R. China, and Graduate School of the Chinese Academy of Sciences, Beijing 100039, P.R. China

Received January 24, 2008

Nine members of a new anions-controlled Cd(II)-guanazole (3,5-diamino-1,2,4-triazole = Hdatrz) hybrid family, that is, $[Cd_3(datrz)_6(H_2O)_2]$ (**1**), $[Cd_3(datrz)_4F_2]$ (**2**), $[Cd_5(datrz)_4Cl_4(OH)_2]$ (**3**), $[Cd_5(datrz)_4Br_4(OH)_2]$ (**4**), $[Cd_3(datrz)_2(SO_3)_2]\cdot(H_2O)$ (**5**), $[Cd_3(datrz)_2(O_2CMe)_4]$ (**6**), [Cd(datrz)(O_2CEt)] (**7**), [Cd(Hdatrz)(O_2C^tBu)$_2$] (**8**), and $[Cd(Hdatrz)_2(H_2Edta)]$ (**9**) have been synthesized by exploiting hydrothermal reactions of guanazole with suitable cadmium salts under appropriate reaction conditions. With effective control of inorganic or organic anions, the coordination diversity of the guanazole ligand in **1**−**9** manifests an unprecedented enrichment with five bridging modes varying from bidentate to quadridentate, two of which are first reported. Compound **1** is the first reported three-dimensional chiral complex constructed from the guanazole ligand which adopts a novel N1, N2, amino N-bridging mode. Halogen anions F^-, Cl^-, and Br^- controlled compounds **2**−**4** are all three-dimensional, with their guanazole ligands possessing another novel quadridentate bridging mode. Sulfite anions controlled compound **5** displays a three-dimensional network with peculiar cage-like hexnuclear cadmium clusters. As for organic anions, low dimensional structures have been found for alkylcarboxylate anions $MeCO_2^-$, $EtCO_2^-$, and $^tBuCO_2^-$ controlled compounds **6**, **7**, and **8** (two-dimensional) and for H_2Edta^{2-} controlled compound **9** (zero- dimensional), and their guanazole ligands manifest low coordination numbers as well. These hybrid materials also present interesting structure-induced physical properties. The chiral compound **1** exhibits the second-order nonlinear optical properties at room temperature. Compounds **2**−**9** except **6** all exhibit photoluminescence of blue fluorescent emissions in the solid state at ambient temperature, which may be assigned to the intraligand $\pi-\pi^*$ transitions. Some structure related red or blue emission shifts have been investigated. Thermal studies show that most compounds of this study possess a high thermal stability.

Introduction

The design and synthesis of coordination polymers from metal ions and organic ligands have been flourishing during recent years because of their intriguing architectures, new topologies, and potential applications as new hybrid materials.[1−3] Such materials are endowed with a range of physical properties giving rise to applications in areas as diverse as gas storage, sorption, catalysis, magnetics, optics, microelectronics, and biology.[4] Although a variety of metal coordination polymers have been successfully synthesized, true rational control in constructing polymers with desired physical properties still remains a distant prospect in crystal engineering.[5]

To date, a large number of coordination polymers, which have been extensively investigated, are assembled from polycarboxylate and polypyridine ligands.[6] Polypyridines can

* To whom correspondence should be addressed. E-mail: yyg@fjirsm.ac.cn. Fax: +86-591-83714946. Telephone: +86-591-83711523.

† Fujian Institute of Research on the Structure of Matter, The Chinese Academy of Sciences.

‡ Graduate School of the Chinese Academy of Sciences.

(1) (a) Chui, S. S. Y.; Lo, S. M. F.; Charmant, J. P. H.; Orpen, A. G.; Williams, I. D. *Science* **1999**, *283*, 1148. (b) Coronado, E.; Galan-Mascaros, J. R.; Gomez-Garcia, C. J.; Laukhin, V. *Nature* **2000**, *408*, 447. (c) Halder, G. J.; Kepert, C. J.; Moubaraki, B.; Murray, K. S.; Cashion, J. D. *Science* **2002**, *298*, 1762. (d) Kim, J.; Jung, I. S.; Kim, S. Y.; Lee, E.; Kang, J. K.; Sakamoto, S.; Yamaguchi, K.; Kim, K. *J. Am. Chem. Soc.* **2000**, *122*, 540. (e) Lightfoot, P.; Mehta, M. A.; Bruce, P. G. *Science* **1993**, *262*, 883. (f) Matsui, S.; Mitani, M.; Saito, J.; Tohi, Y.; Makio, H.; Matsukawa, N.; Takagi, Y.; Tsuru, K.; Nitabaru, M.; Nakano, T.; Tanaka, H.; Kashiwa, N.; Fujita, T. *J. Am. Chem. Soc.* **2001**, *123*, 6847.

10.1021/ic8001042 CCC: $40.75
Published on Web 05/02/2008

provide more predictable coordination modes than carboxylic acids, and therefore, they have been more frequently used to design and construct finite architectures with coordination satisfied metal cations. However, some limitations of pyridine-type ligands make them unable to afford different charge-balancing requirements and diverse functional group orientations. From the crystal engineering and structural predictability point of view, the most appropriate targets should be the simple topologies by use of small and simple ligands with fewer components. Therefore, five-membered heterocycles of imidazole, pyrazole, triazole, and tetrazole as well as their derivatives are representative and significant for their wide use as bridging ligands in neutral or anionic forms.[7,8] One of such ligands, 1,2,4-triazole can bridge to two metal centers in a neutral form, or in a trazolate form can bridge to three metal centers, and exhibits an extensively documented ability to bridge metal ions to afford polynuclear compounds.[9–11] These compounds display extraordinary structural diversity and facile accessibility of functionalized new materials. As reported by Kahn et al.,[12] the superexchange capacity of 1,2,4-triazole endows the remarkable magnetic properties to iron phase complexes.

Even though a variety of coordination polymers with 3,5-disubsituted 1,2,4-triazoles as ligands bridging to transition metal centers have been reported,[13] only a few complexes of guanazole (3,5-diamino-1,2,4-triazole = Hdatrz) ligand have been documented to date.[14–24] Because of this scarcity, the rich coordination chemistry of this ligand needs to be investigated thoroughly.

Scheme 1

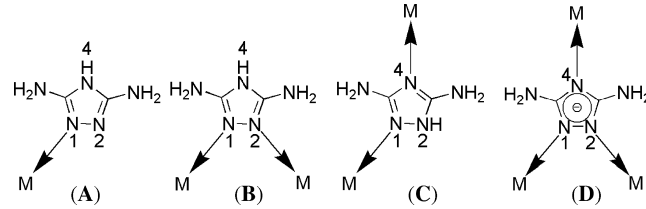

Scheme 2

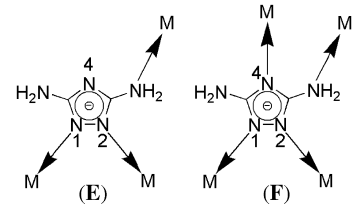

The guanazole ligand is generally considered as bridging to metal centers in four different ways (Scheme 1): (**A**) monodentate N1/N2-bridging mode; (**B**) bidentate N1, N2-bridging mode; (**C**) bidendate N1/N2, N4-bridging mode; (**D**) tridentate N1, N2, N4-bridging mode (with deprotonation at N4 site). Besides these modes, two novel coordination types have been first discovered in this study, that is, (**E**) tridentate N1, N2, amino N-bridging mode; (**F**) quadridentate N1, N2, N4, amino N-bridging mode (Scheme 2). Thus, it is noteworthy that the guanazole ligand can provide quite a structural diversity, which is able to be effectively imprinted onto the metal coordination centers, affording versatile and structural tunable inorganic-organic hybrid materials.

It is known that inorganic or organic counteranions can effectively induce the coordination versatility of the organic ligand, and thus, influence the architectures and physical properties of coordination polymers. By means of this inducement, assembling of structure-predictable complexes

(2) (a) Reineke, T. M.; Eddaoudi, M.; Fehr, M.; Kelley, D.; Yaghi, O. M. *J. Am. Chem. Soc.* **1999**, *121*, 1651. (b) Subramanian, S.; Zaworotko, M. J. *Angew. Chem., Int. Ed. Engl.* **1995**, *34*, 2127. (c) Yaghi, O. M.; O'Keeffe, M.; Ockwig, N. W.; Chae, H. K.; Eddaoudi, M.; Kim, J. *Nature* **2003**, *423*, 705. (d) Power, K. N.; Hennigar, T. L.; Zaworotko, M. J. *Chem. Commun.* **1998**, 595. (e) Zhang, J.; Bu, X. H. *Angew. Chem., Int. Ed.* **2007**, *46*, 6115. (f) Zhang, J.; Liu, R.; Feng, P. Y.; Bu, X. H. *Angew. Chem., Int. Ed.* **2007**, *46*, 8388. (g) Zhang, J.; Yao, Y. G.; Bu, X. H. *Chem. Mater.* **2007**, *19*, 5083. (h) Zhang, J.; Chen, S. M.; Valle, H.; Wong, M.; Austria, C.; Cruz, M.; Bu, X. H. *J. Am. Chem. Soc.* **2007**, *129*, 14168.

(3) (a) Carlucci, L.; Ciani, G.; Macchi, P.; Proserpio, D. M. *Chem. Mater.* **1998**, 1837. (b) Carlucci, L.; Ciani, G.; Proserpio, D. M.; Porta, F. *Angew. Chem., Int. Ed.* **2003**, *42*, 317. (c) Guan, Z. B.; Cotts, P. M.; McCord, E. F.; McLain, S. J. *Science* **1999**, *283*, 2059. (d) Zheng, S. L.; Tong, M. L.; Chen, X. M. *Coord. Chem. Rev.* **2003**, *246*, 185.

(4) (a) Dinca, M.; Long, J. R. *J. Am. Chem. Soc.* **2005**, *127*, 9376. (b) Kitaura, R.; Seki, K.; Akiyama, G.; Kitagawa, S. *Angew. Chem., Int. Ed.* **2003**, *42*, 428. (c) Murray, K. S.; Kepert, C. J. *Spin Crossover Transition Met. Compd. I* **2004**, *233*, 195. (d) Deronzier, A.; Moutet, J. C. *Coord. Chem. Rev.* **1996**, *147*, 339. (e) Smith, R. C.; Tennyson, A. G.; Lippard, S. J. *Inorg. Chem.* **2006**, *45*, 6222.

(5) Robson, R. *J. Chem. Soc., Dalton Trans.* **2000**, 3735.

(6) (a) Hurley, D. J.; Tor, Y. *J. Am. Chem. Soc.* **2002**, *124*, 3749. (b) Mamula, O.; von Zelewsky, A. *Coord. Chem. Rev.* **2003**, *242*, 87. (c) McClenaghan, N. D.; Passalacqua, R.; Loiseau, F.; Campagna, S.; Verheyde, B.; Hameurlaine, A.; Dehaen, W. *J. Am. Chem. Soc.* **2003**, *125*, 5356. (d) McMillin, D. R.; Moore, J. J. *Coord. Chem. Rev.* **2002**, *229*, 113. (e) Pal, S. *J. Chem. Soc., Dalton Trans.* **2002**, 2102.

(7) (a) Chivers, T.; Fu, Z. Y.; Thompson, L. K. *Chem. Commun.* **2005**, 2339. (b) Du, M.; Jiang, X. J.; Zhao, X. J. *Chem. Commun.* **2005**, 5521. (c) Ferrer, S.; Lloret, F.; Bertomeu, I.; Alzuet, G.; Borras, J.; Garcia-Granda, S.; Liu-Gonzalez, M.; Haasnoot, J. G. *Inorg. Chem.* **2002**, *41*, 5821. (d) Klingele, M. H.; Brooker, S. *Coord. Chem. Rev.* **2003**, *241*, 119.

(8) (a) Zhang, J. P.; Chen, X. M. *Chem. Commun.* **2006**, 1689. (b) Zhang, J. P.; Lin, Y. Y.; Huang, X. C.; Chen, X. M. *J. Am. Chem. Soc.* **2005**, *127*, 5495. (c) Zhang, J. P.; Lin, Y. Y.; Zhang, W. X.; Chen, X. M. *J. Am. Chem. Soc.* **2005**, *127*, 14162. (d) Zhang, J. P.; Zheng, S. L.; Huang, X. C.; Chen, X. M. *Angew. Chem., Int. Ed.* **2004**, *43*, 206.

(9) Ouellette, W.; Galan-Mascaros, J. R.; Dunbar, K. R.; Zubieta, J. *Inorg. Chem* **2006**, *45*, 1909.

(10) Ouellette, W.; Hudson, B. S.; Zubieta, J. *Inorg. Chem.* **2007**, *46*, 4887.

(11) Ouellette, W.; Prosvirin, A. V.; Chieffo, V.; Dunbar, K. R.; Hudson, B.; Zubieta, J. *Inorg. Chem.* **2006**, *45*, 9346.

(12) Kahn, O.; Martinez, C. J. *Science* **1998**, *279*, 44.

(13) (a) Beckmann, U.; Brooker, S. *Coord. Chem. Rev.* **2003**, *245*, 17. (b) Haasnoot, J. G. *Coord. Chem. Rev.* **2000**, *200*, 131.

(14) Antolini, L.; Fabretti, A. C.; Gatteschi, D.; Giusti, A.; Sessoli, R. *Inorg. Chem.* **1991**, *30*, 4858.

(15) Fabretti, A. C. *J. Crystallogr. Spectrosc. Res.* **1992**, *22*, 523.

(16) Fabretti, A. C.; Giusti, A.; Sessoli, R. *Inorg. Chim. Acta* **1993**, *205*, 53.

(17) Grap, S. R.; Kuzmina, L. G.; Burtseva, O. Y.; Poraikoshits, M. A.; Kurbakova, A. P.; Efimenko, I. A. *Zh. Neorg. Khim.* **1991**, *36*, 1427.

(18) Grap, S. R.; Kuzmina, L. G.; Poraikoshits, M. A.; Kurbakova, A. P.; Efimenko, I. A. *Koord. Khim.* **1993**, *19*, 566.

(19) Zhai, Q. G.; Lu, C. Z.; Chen, S. M.; Xu, X. J.; Yang, W. B. *Inorg. Chem. Commun.* **2006**, *9*, 819.

(20) Antolini, L.; Fabretti, A. C.; Gatteschi, D.; Giusti, A.; Sessoli, R. *Inorg. Chem.* **1990**, *29*, 143.

(21) Desseyn, H. O.; Fabretti, A. C.; Malavasi, M. *J. Crystallogr. Spectrosc. Res.* **1990**, *20*, 355.

(22) Zhai, Q. G.; Wu, X. Y.; Chen, S. M.; Lu, C. Z.; Yang, W. B. *Cryst. Growth Des.* **2006**, *6*, 2126.

(23) Zhang, G. F.; Zhao, S. M.; She, J. B.; Ng, S. W. *Acta Crystallogr. Sect. E: Struct. Rep. Online* **2006**, *62*, M2148.

(24) Aznar, E.; Ferrer, S.; Borras, J.; Lloret, F.; Liu-Gonzalez, M.; Rodriguez-Prieto, H.; Garcia-Granda, S. *Eur. J. Inorg. Chem.* **2006**, 5115.

can be controlled via designed selection of appropriate inorganic or organic counteranions in a metal−organic hybrid system. However, to the best of our knowledge, the systematical investigation of anion-controlled coordination versatility of the organic ligand in the construction of complexes is rarely known.

Herein, we report a comprehensive study of a new Cd(II)-guanazole (3,5-diamino-1,2,4-triazole = Hdatrz) hybrid family with unprecedented structural diversity, which is effectively controlled by various inorganic or organic anions. Nine novel materials with a general scheme of Cd(II)/datrz(or Hdatrz)/X have been prepared with X = H_2O, F^-, Cl^-, Br^-, SO_3^{2-}, $MeCO_2^-$, $EtCO_2^-$, $^tBuCO_2^-$, and H_2Edta^-, respectively (H_4Edta is the ethylenediaminetetraacetate). To the best of our knowledge, only three X-ray structures of the guanazole with Cd(II) have been reported previously.[21–23] The structure of $[Cd_3(datrz)_6(H_2O)_2]$ (**1**), $[Cd_3(datrz)_4F_2]$ (**2**), $[Cd_5(datrz)_4Cl_4(OH)_2]$ (**3**), $[Cd_5(datrz)_4Br_4(OH)_2]$ (**4**), $[Cd_3(datrz)_2(SO_3)_2]\cdot(H_2O)$ (**5**), $[Cd_3(datrz)_2(O_2CMe)_4]$ (**6**), [Cd(datrz)(O2CEt)] (**7**), $[Cd(Hdatrz)(O_2C^tBu)_2]$ (**8**), and $[Cd(Hdatrz)_2(H_2Edta)]$ (**9**) are reported, and their structure induced physical properties, like thermal stability, photoluminescence, and so forth, are also described and discussed.

Experimental Section

General Considerations. Commercially available reagents were used as received without further purification. All syntheses were carried out in 23 mL poly(tetrafluoroethylene) lined stainless steel containers under autogenous pressure. The elemental analyses were performed on an EA1110 CHNS-0 CE elemental analyzer. The IR spectroscopy was recorded on a PECO (U.S.A.) SpectrumOne spectrophotometer with pressed KBr pellets. Thermal stability studies were carried out on a NETSCHZ STA-449C thermoanalyzer. The thermal decomposition behavior of **5** was analyzed by thermogravimetric analysis mass spectrometry (TGA-MS) using the NETSCH STA-449C thermoanalyzer coupled with a NETSCH QMS403C mass spectrometer. The fluorescence spectra were measured on polycrystalline or powder samples at room temperature using an Edinburgh FLS920 TCSPC fluorescence spectrophotometer. The phase purity and crystallinity of each product were checked by powder X-ray diffraction (XRD) analysis using a Rigaku Dmax2500 diffractometer with Cu Kα radiation ($\lambda = 1.54056$ Å). A step size of 0.05° and counting time of 1.2 s/step were applied in a 2θ range of 5.00−55.00°. The observed and simulated powder XRD patterns of all compounds are displayed in Supporting Information, Figure S1.

Synthesis of $[Cd_3(datrz)_6(H_2O)_2]$ (1). A mixture of Hdatrz (0.1 g, 1.0 mmol), $CdCl_2\cdot 2.5H_2O$ (0.136 g, 0.6 mmol) and aqueous ammonia (25%, 2.0 mL) was placed in a 23 mL Teflon liner; 2 mL of ethanol and 8 mL of water were then added. The resulting suspension was stirred for 5 min and was then sealed in a Parr autoclave. The autoclave was placed in a programmable furnace and heated to 160 °C. The temperature was held for 3 days, and then, the reactant mixture was cooled at a rate of 0.5 °C min^{-1} to form colorless prism crystals of **1**. Yield: 78%. Anal. Calcd (%) for $C_{12}H_{28}Cd_3N_{30}O_2$: C, 14.99; H, 2.93; N, 43.69. Found: C, 15.02; H, 2.91; N, 43.72%. IR (solid KBr pellet, υ/cm^{-1}) for complex **1**: 3435 (s), 3193 (s), 1627 (m), 1528 (w), 1489 (w), 1469 (w), 1400 (m), 1162 (w), 893 (w), 670 (w), 614 (w).

Synthesis of $[Cd_3(datrz)_4F_2]$ (2). The reaction was carried out in a procedure similar to that for **1**, using $Cd(MeCO_2)_2\cdot 2H_2O$ (0.1 g, 0.37 mmol) and NaF (0.042 g, 1.0 mmol) instead of $CdCl_2\cdot 2.5H_2O$ and aqueous ammonia. Colorless block crystals of **2** were isolated in 90% yield. Anal. Calcd (%) for $C_8H_{16}Cd_3F_2N_{20}$: C, 12.52; H, 2.10; N, 36.50; F, 4.95. Found: C, 12.56; H, 2.14; N, 36.47; F, 4.89%. IR (solid KBr pellet, υ/cm^{-1}) for complex **2**: 3438 (m), 3402 (m), 3197 (br, m), 1615 (m), 1557 (m), 1486 (m), 1399 (m), 1153 (w), 1077 (w), 1019 (w), 825 (w), 763 (w), 615 (w).

Synthesis of $[Cd_5(datrz)_4Cl_4(OH)_2]$ (3). The reaction was carried out in a procedure similar to that for **1**, only using $CdCl_2\cdot 2.5H_2O$ (0.136 g, 0.6 mmol) and Hdatrz (0.1 g, 1.0 mmol) without aqueous ammonia. Light yellow prism crystals of **3** were isolated in 56% yield. Anal. Calcd (%) for $C_8H_{18}Cd_5Cl_4N_{20}O_2$: C, 8.50; H, 1.61; N, 24.79; Cl, 12.55. Found: C, 8.51; H, 1.58; N, 24.47; Cl, 12.49%. IR (solid KBr pellet, υ/cm^{-1}) for complex **3**: 3414 (m), 3333 (m), 3178 (m), 1619 (m), 1500 (w), 1465 (w), 1401 (m), 1157 (w), 1091 (w), 937 (w), 817 (w), 749 (w), 614 (w).

Synthesis of $[Cd_5(datrz)_4Br_4(OH)_2]$ (4). The reaction was carried out in a procedure similar to that for **3**, using $CdBr_2\cdot 4H_2O$ (0.172 g, 0.5 mmol) instead of $CdCl_2\cdot 2.5H_2O$. Light yellow block crystals of **4** were isolated in 70% yield. Anal. Calcd (%) for $C_8H_{18}Br_4Cd_5N_{20}O_2$: C, 7.35; H, 1.39; N, 21.42; Br, 24.43. Found: C, 7.38; H, 1.42; N, 21.38; Br, 24.36%. IR (solid KBr pellet, υ/cm^{-1}) for complex **4**: 3413 (s), 3349 (s), 3278 (s), 3182 (s), 1667 (m), 1625 (m), 1579 (m), 1548 (m), 1498 (m), 1403 (m), 1108 (m), 988 (w), 825 (w), 763 (w), 709 (w), 616 (w).

Synthesis of $[Cd_3(datrz)_2(SO_3)_2]\cdot(H_2O)$ (5). The reaction was carried out in a procedure similar to that for **3**, using $Cd(NO_3)_2\cdot 4H_2O$ (0.154 g, 0.5 mmol) and sodium sulfite (0.126 g, 1.0 mmol) instead of $CdCl_2\cdot 2.5H_2O$. Colorless rod crystals of **5** were isolated in 55% yield. Anal. Calcd (%) for $C_4H_{10}Cd_3N_{10}O_7S_2$: C, 6.75; H, 1.42; N, 19.69. Found: C, 6.71; H, 1.40; N, 19.72%. IR (solid KBr pellet, υ/cm^{-1}) for complex **5**: 3434 (s), 3173 (m), 1628 (m), 1400 (s), 1160 (m), 1091 (w), 877 (w), 635 (w), 614.11 (w).

Synthesis of $[Cd_3(datrz)_2(O_2CMe)_4]$ (6). The reaction was carried out in a procedure similar to that for **3**, using $Cd(MeCO_2)_2\cdot 2H_2O$ (0.134 g, 0.5 mmol) instead of $CdCl_2\cdot 2.5H_2O$. Colorless block crystals of **6** were isolated in 85% yield. Anal. Calcd (%) for $C_{12}H_{20}Cd_3N_{10}O_8$: C, 18.73; H, 2.62; N, 18.20. Found: C, 18.70; H, 2.63; N, 18.24%. IR (solid KBr pellet, υ/cm^{-1}) for complex **6**: 3428 (m), 3349 (m), 3230 (m), 1634 (m), 1579 (m), 1498 (m), 1403 (s), 1156 (w), 1072 (w), 1018 (w), 949 (w), 835 (w), 754 (w), 678 (w), 626 (w).

Synthesis of $[Cd(datrz)(O_2CEt)]$ (7). The reaction was carried out in a procedure similar to that for **3**, using $Cd(NO_3)_2\cdot 4H_2O$ (0.308 g, 1.0 mmol) and sodium propionate (0.096 g, 1.0 mmol) instead of $CdCl_2\cdot 2.5H_2O$. Colorless block crystals of **7** were isolated in 85% yield. Anal. Calcd (%) for $C_5H_9CdN_5O_2$: C, 21.18; H, 3.20; N, 24.70. Found: C, 21.16; H, 3.24; N, 24.68%. IR (solid KBr pellet, υ/cm^{-1}) for complex **7**: 3456 (m), 3343 (m), 2976 (w), 1626 (m), 1565 (s), 1466 (m), 1399 (m), 1296 (m), 1059 (w), 896 (w), 814 (w), 757 (w), 677 (w).

Synthesis of $[Cd(Hdatrz)(O_2C^tBu)_2]$ (8). The reaction was carried out in a procedure similar to that for **3**, using $Cd(NO_3)_2\cdot 4H_2O$ (0.308 g, 1.0 mmol) and pivalic acid (0.102 g, 1.0 mmol) instead of $CdCl_2\cdot 2.5H_2O$. Colorless column crystals of **8** were isolated in 85% yield. Anal. Calcd (%) for $C_{12}H_{23}CdN_5O_4$: C, 34.84; H, 5.56; N, 16.93. Found: C, 34.85; H, 5.55; N, 16.90%. IR (solid KBr pellet, υ/cm^{-1}) for complex **8**: 3391 (s), 3322 (s), 3162 (s), 2962 (m), 1640 (m), 1541 (s), 1485 (m), 1414 (m), 1225 (w), 1077 (w), 902 (w), 794 (w), 748 (w), 605 (w).

Synthesis of $[Cd(Hdatrz)_2(H_2Edta)]$ (9). The reaction was carried out in a procedure similar to that for **3**, using

Table 1. Crystal Data and Structure Refinements for Compounds **1**−**9**

param	1	2	3	4	5
formula	$C_{12}H_{28}Cd_3N_{30}O_2$	$C_8H_{16}Cd_3F_2N_{20}$	$C_8H_{18}Cd_5Cl_4N_{20}O_2$	$C_8H_{18}Br_4Cd_5N_{20}O_2$	$C_4H_{10}Cd_3N_{10}O_7S_2$
fw	961.87	767.64	1130.27	1308.07	711.59
temp(*K*)	294.15	294.15	294.15	294.15	294.15
cryst syst	monoclinic	monoclinic	monoclinic	monoclinic	monoclinic
space group	*C*2	$P2_1/c$	$P2_1/c$	$P2_1/c$	$P2_1/c$
a (Å)	12.577(7)	9.326(3)	9.2003(1)	9.285(3)	10.648(9)
b (Å)	15.320(7)	7.865(2)	10.2021(2)	10.399(4)	8.503(7)
c (Å)	8.170(4)	13.129(4)	13.9177(3)	14.001(5)	17.185(15)
α (Å)	90	90	90	90	90
β (Å)	116.062(6)	105.137(3)	94.773(1)	95.642(7)	95.360(13)
γ (Å)	90	90	90	90	90
V (Å^3)	1414.1(12)	929.6(5)	1309.48(4)	1345.3(8)	1549(2)
Z	2	2	2	2	4
D_{calcd} (g cm^{-3})	2.259	2.743	2.867	3.229	3.051
μ (mm^{-1})	2.312	3.472	4.456	9.88	4.411
GOF	1.006	1.032	1.089	1.02	1.050
R1[a] ($I > 2\sigma(I)$)	0.0227	0.0167	0.0298	0.0225	0.0355
wR2[a] (all data)	0.0484	0.0442	0.0773	0.049	0.092

param	6	7	8	9
formula	$C_{12}H_{20}Cd_3N_{10}O_8$	$C_5H_9CdN_5O_2$	$C_{12}H_{23}CdN_5O_4$	$C_{14}H_{24}CdN_{12}O_8$
fw	769.61	283.57	413.75	600.86
temp (K)	294.15	294.15	294.15	294.15
cryst syst	monoclinic	orthorhombic	monoclinic	monoclinic
space group	*C2/c*	*Pccn*	$P2_1/c$	*C2/c*
a (Å)	24.102(9)	18.1526(13)	12.781(3)	24.214(7)
b (Å)	7.134(2)	10.0844(6)	9.887(2)	8.952(2)
c (Å)	13.690(5)	10.1725(7)	14.615(4)	14.770(5)
α (Å)	90	90	90	90
β (Å)	107.420(4)	90	98.286(4)	130.485(4)
γ (Å)	90	90	90	90
V (Å^3)	2246.0(13)	1862.2(2)	1827.6(8)	2133.4(11)
Z	4	8	4	4
D_{calcd} (g cm^{-3})	2.276	2.023	1.504	1.871
μ (mm^{-1})	2.876	2.323	1.217	1.097
GOF	1.012	1.089	1.046	1.008
R1[a] ($I > 2\sigma(I)$)	0.0197	0.0351	0.0417	0.0207
wR2 (all data)	0.0485	0.0918	0.1319	0.0586

[a] $R1 = \sum||F_o| - |F_c||/\sum|F_o|$; $wR2 = \{\sum[w(F_o^2 - F_c^2)^2]/\sum[w(F_o^2)^2]\}^{1/2}$, $w = 1/[\sigma^2(F_o^2) + (aP)^2 + bP]$, where $P = [\max(F_o^2,0) + 2F_c^2]/3$ for all data.

$Cd(NO_3)_2 \cdot 4H_2O$ (0.154 g, 0.5 mmol) and disodium EDTA (0.186 g, 0.5 mmol) instead of $CdCl_2 \cdot 2.5H_2O$. Colorless block crystals of **9** were isolated in 95% yield. Anal. Calcd (%) for $C_{14}H_{24}CdN_{12}O_8$: C, 27.99; H, 4.03; N, 27.97. Found: C, 28.02; H, 4.00; N, 27.92%. IR (solid KBr pellet, υ/cm^{-1}) for complex **9**: 3350 (m), 3109 (m), 1697 (s), 1671 (s), 1579 (s), 1446 (m), 1409 (s), 1354 (m), 1266 (m), 1110 (m), 1041 (w), 973 (w), 933 (w), 858 (w), 807 (w), 722 (m), 651 (w).

X-ray Crystallography. Suitable single crystals of **1**−**9** were carefully selected under an optical microscope and glued to thin glass fibers. Structural measurements were performed on a computer-controlled Siemens Smart CCD diffractometer with graphite-monochromated Mo Kα radiation ($\lambda_{Mo\ K\alpha} = 0.71073$ Å) at $T =$ 294.15 K. Absorption corrections were made using the SADABS program.[25] The structures were solved using the direct method and refined by full-matrix least-squares methods on F^2 by using the SHELX-97 program package.[26] All non-hydrogen atoms except those needed for disorder modeling were refined anisotropically, and hydrogen atoms attached to carbon or nitrogen atoms were fixed at their ideal positions. The water or hydroxyl hydrogen atoms were located from difference maps and refined with isotropic temperature factors. Disorders were observed for the C atoms of the *tert*-butyl groups in **8**, and they were refined over two sites with occupancies of 0.516(11) and 0.484(11), respectively. Crystal data and refinement of **1**−**9** are summarized in Table 1. Selected bond lengths and angles are given in Supporting Information, Table S1.

(25) Sheldrick, G. M. *SADABS, Program for Area Detector Adsorption Correction*; Institute for Inorganic Chemistry, University of Göttingen: Göttingen, Germany, 1996.

(26) Sheldrick, G. M. *SHELXL-97, Program for Solution of Crystal Structures*; University of Göttingen: Göttingen, Germany, 1997.

Results and Discussion

Synthesis and Infrared Spectroscopy. It is known that the product composition depends on critical factors such as the ratio between metal salts and ligands, pH value, temperature, reaction time, as well as the charge-balancing anions. By exploitation of the hydrothermal reactions, all compounds were synthesized in good yields using guanazole ligands and suitable cadmium salts. In this contribution, it is noticeable that there are two crucial factors that govern the formation of final products: one is the pH value, and the other is the cadmium source. In our experiments, the pH values were kept at 6.0−6.5 for **2**, **3**, **4**, **5**, **8**, and **9** and at 5.0−5.5 for **6**, and **7**. When the pH value was adjusted above 8.0 (using 25% aqueous ammonia), all products obtained were colorless prism crystals uniquely, that is, the chiral compound **1**. In other words, inorganic or organic anions could not be incorporated into the complex in an alkaline environment in which cadmium cations are charge-balanced by deprotonated guanazolate ligands solely.

The selection of suitable cadmium salts is the second crucial factor in synthesizing these materials. The chemistry of cadmium guanazolates is generally characterized by incorporating anionic components of metal salts into the final compounds. An exception is that, through many repeat experiments, it failed to incorporate the nitrate anions of $Cd(NO_3)_2 \cdot 4H_2O$ into the final product to provide the anticipated Cd/datrz/NO_3^- phase. Thanks to this phenomenon, $Cd(NO_3)_2 \cdot 4H_2O$ was chosen as the starting material which could afford Cd^{2+} ions exclusively, and by means of this cadmium salt, selected inorganic or organic anions (SO_3^{2-}, $EtCO_2^-$, $^tBuCO_2^-$, and H_2Edta^-) could be incorporated into the final products, affording the desired compounds $[Cd_3(datrz)_2(SO_3)_2] \cdot (H_2O)$ (**5**), $[Cd(datrz)(O_2CEt)]$ (**7**), $[Cd(Hdatrz)(O_2C^tBu)_2]$ (**8**), and $[Cd(Hdatrz)_2(H2Edta)]$ (**9**).

The infrared spectra of all compounds exhibit a medium to strong intensity band in the 3100−3460 cm^{-1} range: 3100−3236 cm^{-1} associated with $\upsilon_s(N-H)_{NH,NH2}$, 3310−3400 cm^{-1} associated with $\upsilon_{as}(N-H)_{NH,NH2}$ of the guanazole ligand, and 3410−3460 cm^{-1} associated with $\upsilon(N-H)_{NH,NH2}$ plus $\upsilon(O-H)_{H2O}$. Besides these, a medium to strong band in the 1615−1680 cm^{-1} range and a medium band in the 1400−1488 cm^{-1} range are also observed, both of them associated with $\upsilon(C{=}N)$/ring stretching vibrations plus $\delta(N-H)_{NH,NH2}$ of the guanazole ligand. The IR spectrum of guanazole has already been studied in detail by Desseyn et al.[21]

Chiral 3D Connectivity in $[Cd_3(datrz)_6(H_2O)_2]$ (1). X-ray crystallographic analysis reveals that compound **1** crystallizes in the chiral space group *C*2. The chiral source of this compound comes from the asymmetrical coordination of Cd1 site, which possesses a C_2 symmetry operation and adopts a distorted trigonal bipyramidal geometry $\{CdN_3(H_2O)_2\}$ with a value of 0.77 for the parameter τ,[27] as shown in Figure 1a,b. This geometry is defined by one N4 nitrogen site from a guanazolate ligand, two symmetry-related amino nitrogen donors, and two symmetry-related aqua ligands. All these asymmetrical Cd1 sites exhibit the same absolute conformation, which gives out a homochiral form,[28] and thus induce chirality into the final framework of the title compound, affording a chiral three-dimensional (3D) network.

The 3D structure of **1** can be considered as $\{Cd_2(datrz)_6\}_n^{n-}$ chains parallel to the *c*-axis bridged through Cd1 sites, as illustrated in Figure 1c,d. Every $\{Cd_2(datrz)_6\}$ unit on the chain consists of two distinct $\{Cd(datrz)_3\}$ subunits, one of which has three guanazolate ligands that only possess the N1, N2-bridging mode (type **B** in Scheme 1). These subunits serve as building blocks to elongate every single chain. Three guanazolate ligands of another $\{Cd(datrz)_3\}$ subunit manifest two kinds of coordination mode: one ligand adopting the N1, N2, N4-bridging mode (type **D** in Scheme 1), and the other two adopting a novel N1, N2, amino N-bridging mode (type **E** in Scheme 2). When the chain is viewed along the *c*-axis, each of the six guanazolate ligands projects outward from the Cd···Cd axis of the chain, with an angle of 60° between the planes of alternate guanazolate rings, obtaining a six-bladed paddle wheel like structure, as shown in Figure 1d.

It is noticeable that the bridging mode **E** has never been reported in coordination modes of the guanazole ligand previously, so its structural diversity is enriched further. In addition, it is known that most of the chiral coordination compounds are synthesized by using chiral organic linkers or chiral metal complexes as second building blocks, and very few 3D chiral coordination polymers based on achiral symmetrical ligands have been reported. This scarcity is generally attributed to that the coordination of the achiral symmetrical ligands often generates racemic asymmetrical coordination centers.[28b] To the best of our knowledge, there is no report about the chiral complex which is constructed from the guanazole ligand to date. However, from this contribution we conclude that under the appropriate experimental condition (when the pH value was adjusted above 8.0), the coordination versatility of the symmetrical guanazole ligand can provide the asymmetrical bridging to the cadmium center and crystallize these centers into a homochiral 3D network. Thus, this study suggests a promising approach to synthesize novel chiral and noncentrosymmetric coordination compounds with intriguing properties, and the chiral compound **1** is the first case.

F^- Ions Controlled 3D Connectivity In $[Cd_3(datrz)_4F_2]$ (2). The structure of fluoride phase $[Cd_3(datrz)_4F_2]$ (**2**) is 3D, and it exhibits two distinct cadmium sites, as shown in Figure 2a. One is a six-coordinate, distorted octahedral $\{CdN_5F\}$ site, with its equatorial plane defined by a μ_2-fluoride ligand, a guanazolate N4 nitrogen donor, and two guanazolate N1 (N2) donors, and its axial sites occupied by an amino nitrogen atom (Cd−N distance is 2.68 Å) and another guanazolate N1 (N2) nitrogen atom. The other cadmium site also adopts an octahedral geometry $\{CdN_4F_2\}$, defined by four equatorial guanazolate nitrogens and two axial μ_2-fluoride ligands. These cadmium sites are connected by guanazolate and μ_2-fluoride ligands in the transoid disposition, forming a chain-like substructure, which may be understood as octahedral $\{CdN_4F_2\}$ centers bridged by chair-like $\{Cd_2N_4\}$ heterocycles. Adjacent parallel chains are linked to each other to form a corrugated layer structure, as shown in Figure 2b, and these layers are connected through guanazolate ligands that project perpendicularly outward from the layers, affording a complex 3D network, as shown in Figure 2c.

It is noteworthy that half of the guanazolate ligands in **2** adopt the quadridentate N1, N2, N4, amino N-bridging mode (type **F** in Scheme 2), which is another unprecedented coordination mode of the guanazole ligand. Four of all five nitrogen sites of this ligand can bond to metal sites, and it thus shows that the coordination modes of the guanazole

(27) Addison, A. W.; Rao, T. N.; Reedijk, J.; Rijn, J. V.; Verschoor, G. C. *J. Chem. Soc., Dalton Trans.* **1984**, 1349. [A structural index τ for these geometries, which has been defined as $\tau = (\beta - \alpha)/60$, with α and β being the two largest coordination angles. In a perfect square-pyramidal geometry τ is 0, while it is 1 in a perfect trigonal-bipyramidal geometry]

(28) (a) Kesanli, B.; Lin, W. B. *Coord. Chem. Rev.* **2003**, *246*, 305. (b) Evans, O. R.; Lin, W. B. *Acc. Chem. Res.* **2002**, *35*, 511. (c) Evans, O. R.; Wang, Z. Y.; Lin, W. B. *Chem. Commun.* **1999**, 1903. (d) Evans, O. R.; Lin, W. B. *Chem. Mater.* **2001**, *13*, 2705. (e) Zhang, J.; Lin, W.; Chen, Z. F.; Xiong, R. G.; Abrahams, B. F.; Fun, H. K. *Dalton Trans.* **2001**, 1806.

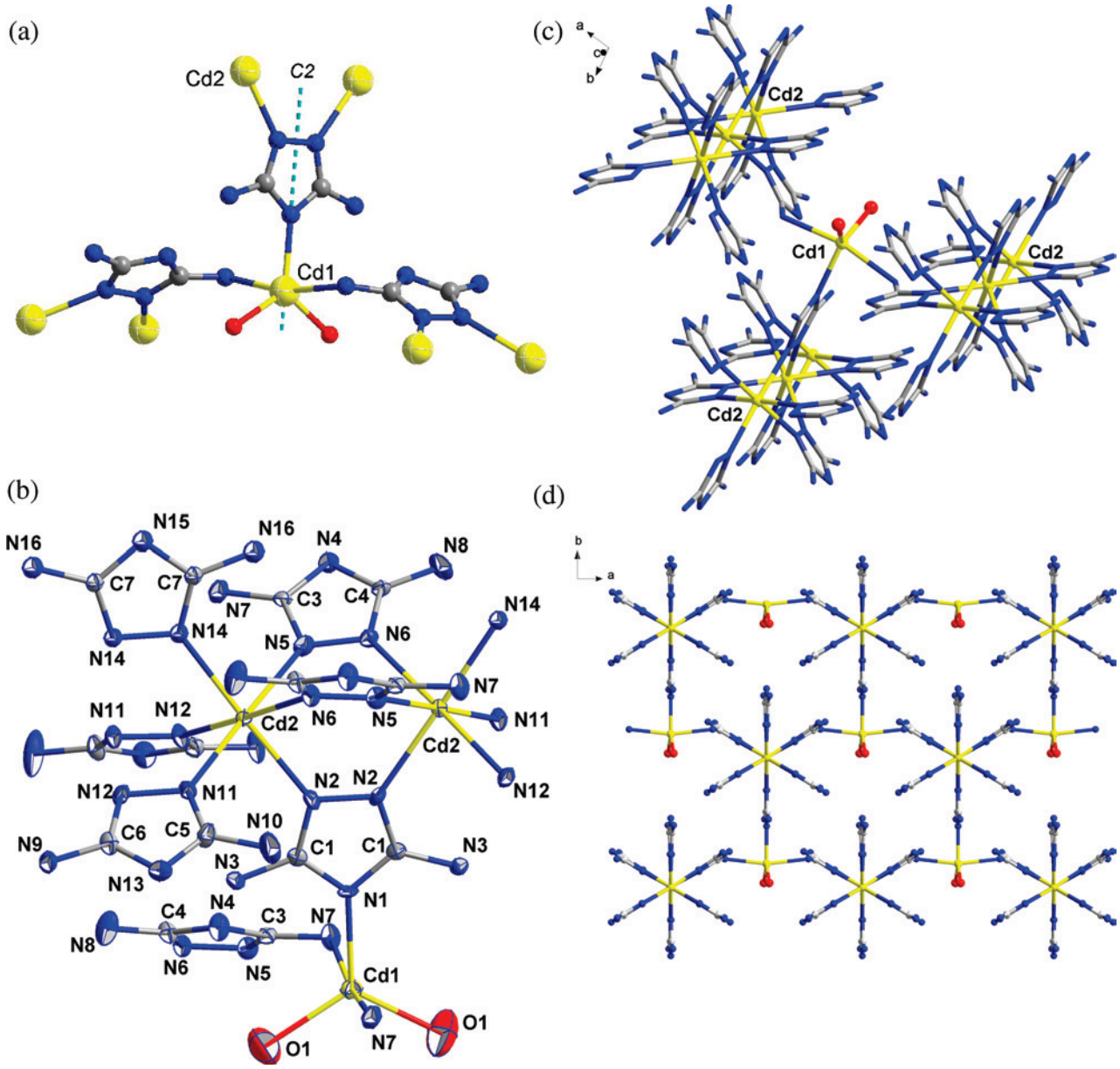

Figure 1. (a) Chiral coordination of the Cd1 site. (b) ORTEP drawing of $[Cd_3(datrz)_6(H_2O)_2]$ (**1**) showing the atom-labeling system and 50% thermal ellipsoids. H atoms have been omitted for clarity. (c) Three $\{Cd_2(datrz)_6\}_n^{n-}$ chains parallel to the *c*-axis bridged through the Cd1 site. (d) View of the 3D structure of **1**.

ligand are beyond commonly encountered bidentate or tridentate mode.

Cl^- or Br^- Ions Controlled 3D Connectivity in $[Cd_5(datrz)_4Cl_4(OH)_2]$ (3) and $[Cd_5(datrz)_4Br_4(OH)_2]$ (4). The chloride phase $[Cd_5(datrz)_4Cl_4(OH)_2]$ (**3**) also exhibits a complex 3D structure (Figure 3c), which manifests three distinct octahedral cadmium sites. As shown in Figure 3a, the first is a $\{CdN_4Cl_2\}$ site, which is defined by four nitrogen donors in the equatorial plane and two axial chloride ligands. The second is a $\{CdN_3Cl_2OH\}$ site, with the equatorial plane occupied by a μ_3-hydroxy ligand, an amino nitrogen donor (Cd−N distance is 2.44 Å), and two N1(N2) nitrogen donors, and its coordination geometry is completed by two μ_2-chloride ligands in the axial positions. The third is a $\{CdN_3Cl(OH)_2\}$ site, defined by a μ_2-chloride ligand, two μ_3-hydroxy ligands, two N4 nitrogen donors, as well as an amino nitrogen donor (Cd−N distance is 2.64 Å). These cadmium sites are linked through guanazolate and hydroxyl ligands, constructing a chain like substructure, which may be described as chair-like $\{Cd_4O_2Cl_2\}$ clusters joined with 2-connected rod-like $\{CdCl_2\}$ knots, as shown in Figure 3b. To our knowledge, this kind of chain structure, which is constructed from pentanuclear cadmium units, is the first example in metal-guanazole/triazole complexes, and the structure of the chair-like $\{Cd_4O_2Cl_2\}$ cluster has never been reported. Similar to **2**, mutually parallel and perpendicular chains of **3** are bridged through guanazolate ligands which all adopt the bridging mode **F** (Scheme 2), producing a complex 3D network with −ABAB− alternations (Figure 3c).

The 3D structure of $[Cd_5(datrz)_4Br_4(OH)_2]$ (**4**) is isomorphous with that of **3**, as shown in Figure 4a. The first difference between **4** and **3** is that the former has Br^- ions with much stronger steric hindrance and longer Cd−Br

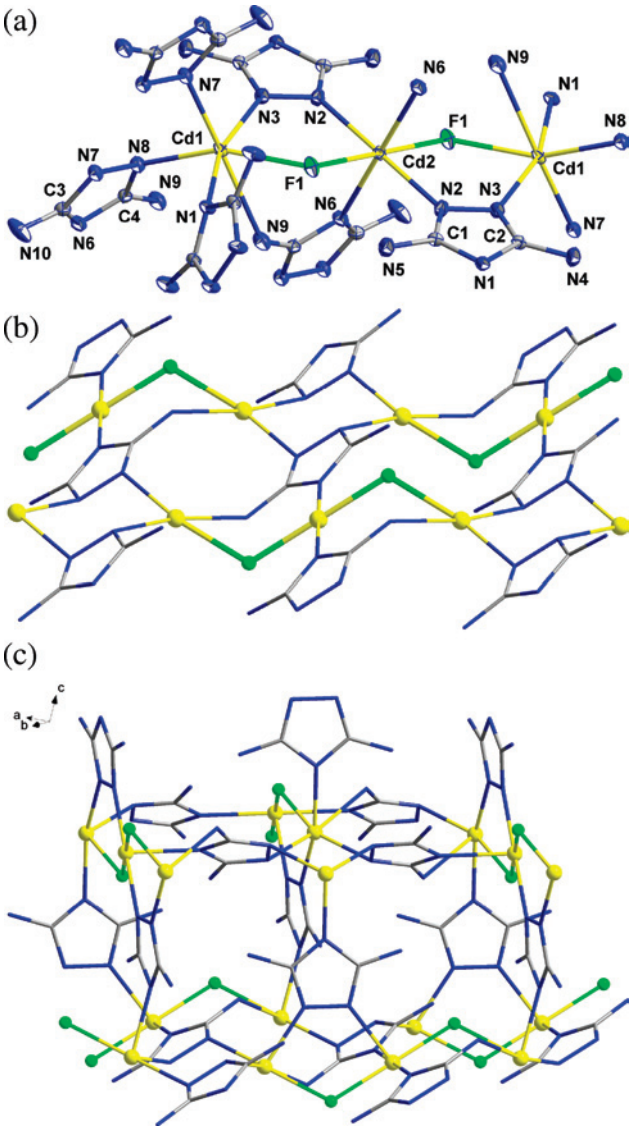

Figure 2. (a) ORTEP drawing of $[Cd_3(datrz)_4F_2]$ (**2**) showing the atom-labeling system and 50% thermal ellipsoids. H atoms have been omitted for clarity. (b) View of the corrugated layer substructure. (c) View of the 3D structure of **2**.

bonds, which lead somewhat to the expansion of its structure, exhibiting an increase in volume (about 2.74%) compared to **3**. Secondly, the structure expansion can significantly influence the bonding interactions between amino nitrogen donors (of the guanazolate ligands) and cadmium centers. In compound **3**, the amino nitrogen donors bond to cadmium centers forming two different bonds, that is, Cd3−N4 bond (2.44 Å) and Cd1−N10 bond (2.64 Å) (Figure 3a), whereas only one bond, that is, Cd2−N10 (2.48 Å) bond, is formed in **4** when its amino nitrogen donors coordinate to cadmium sites. Therefore, the coordination geometry of the Cd3 site in **4** manifests a distorted square pyramid (with the τ value of 0.22), rather than the distorted octahedron in **3**. Similar to **3,** chair-like $\{Cd_4O_2Br_2\}$ clusters of **4** are linked through 2-connected rod-like $\{CdBr_2\}$ knots affording 1D chain substructures, which interweave into a 3D network as shown in Figure 4b.

In addition, half of the guanazolate ligands in Br^- ions controlled compound **4** adopt the bridging mode **F**. Therefore, it is proven that the halogen anions F^-, Cl^-, and Br^- can effectively induce the coordination versatility of the guanazole ligand and control the 3D connectivity of their coordination polymers. By the way, it is reported by Zhai et al that I^- ions can induce the guanazole ligand into adopting the bridging mode **D**, generating a 2D layer structure,[22] so the inducement of the I^- ions is obviously different from that of other halogen anions.

SO_3^{2-} Ions Controlled 3D Connectivity in $[Cd_3(datrz)_2(SO_3)_2(H_2O)]$ (5). The sulfite phase $[Cd_3(datrz)_2(SO_3)_2(H_2O)]$ (**5**) also manifests a complex 3D structure, which can be described as $\{Cd_3(SO_3)_2\}_n^{2n+}$ chains parallel to the *b*-axis linked through the guanazolate ligands, as shown in Figure 5b. The secondary building unit $\{Cd_3(SO_3)_2\}^{2+}$ exhibits three distinct Cd(II) coordination geometries, as shown in Figure 5a. The first is a square pyramidal $\{CdN_2O_3\}$ site ($\tau = 0.02$), with its basal plane occupied by two oxygen atoms from a sulfite group, a N4 nitrogen donor and a N1 (N2) nitrogen donor, and another sulfite oxygen located in the apical position. The second is also a distorted square pyramidal $\{CdN_2O_3\}$ ($\tau = 0.14$), but two oxygen donors in its basal plane come from two different sulfite groups, respectively. The third is a distorted octahedral $\{CdN_2O_4\}$ geometry, which is defined by two guanazolate N1 (N2) nitrogen donors and four sulfite oxygen donors. Two connected $\{Cd_3(SO_3)_2\}^{2+}$ units form a cage like hexnuclear Cd−S−O cluster, which has never been reported to our knowledge, as shown in Figure 5b.

Moreover, there are two kinds of sulfite groups in this complex: one adopting a η^2, μ_5 coordination mode, bridging three square pyramidal and two octahedral cadmium sites, and the other adopting a η^2, μ_4 coordination mode, bridging two square pyramidal and two octahedral cadmium sites. The inorganic $\{Cd_3(SO_3)_2\}_n^{2n+}$ chains are parallel linked by organic guanazolate ligands, each of which adopts the bridging mode **D**, producing a representative inorganic−organic hybrid complex with a 3D network, as shown in Figure 5c.

$MeCO_2^-$ Ions Controlled 2D Connectivity in $[Cd_3(datrz)_2(O_2CMe)_4]$ (6). To investigate the coordination versatility of the guanazole ligand induced by organic anions, three alkylcarboxylate anions $MeCO_2^-$, $EtCO_2^-$, and $^tBuCO_2^-$ with different steric hindrance of their terminal groups (methyl, ethyl, and tertbutyl) are chosen instead of inorganic anions. The acetate phase $[Cd_3(datrz)_2(O_2CMe)_4]$ (**6**) exhibits a two-dimensional (2D) structure (Figure 6b), which has two distinct cadmium geometries. As shown in Figure 6a, the first is constructed from a slightly distorted trigonal prismatic $\{CdN_2O_4\}$ site, which is defined by chelating carboxylate oxygen donors and N4 nitrogen donors. The second is also a $\{CdN_2O_4\}$ site, but interestingly its geometry adopts a distorted octahedron, which is defined by two carboxylate oxygen donors and two N1 (N2) nitrogen donors in the equatorial plane and two μ_2-carboxylate oxygen donors along the axis. These cadmium sites are joined through μ_2-carboxylate oxygen donors, affording a corrugated $\{Cd_3O_4\}_n$ ribbon propagating along the *c*-axis, as shown in Figure 6b.

Parallel ribbons are linked by guanazolate ligands which adopt the bridging mode **D**, generating a 2D layer structure,

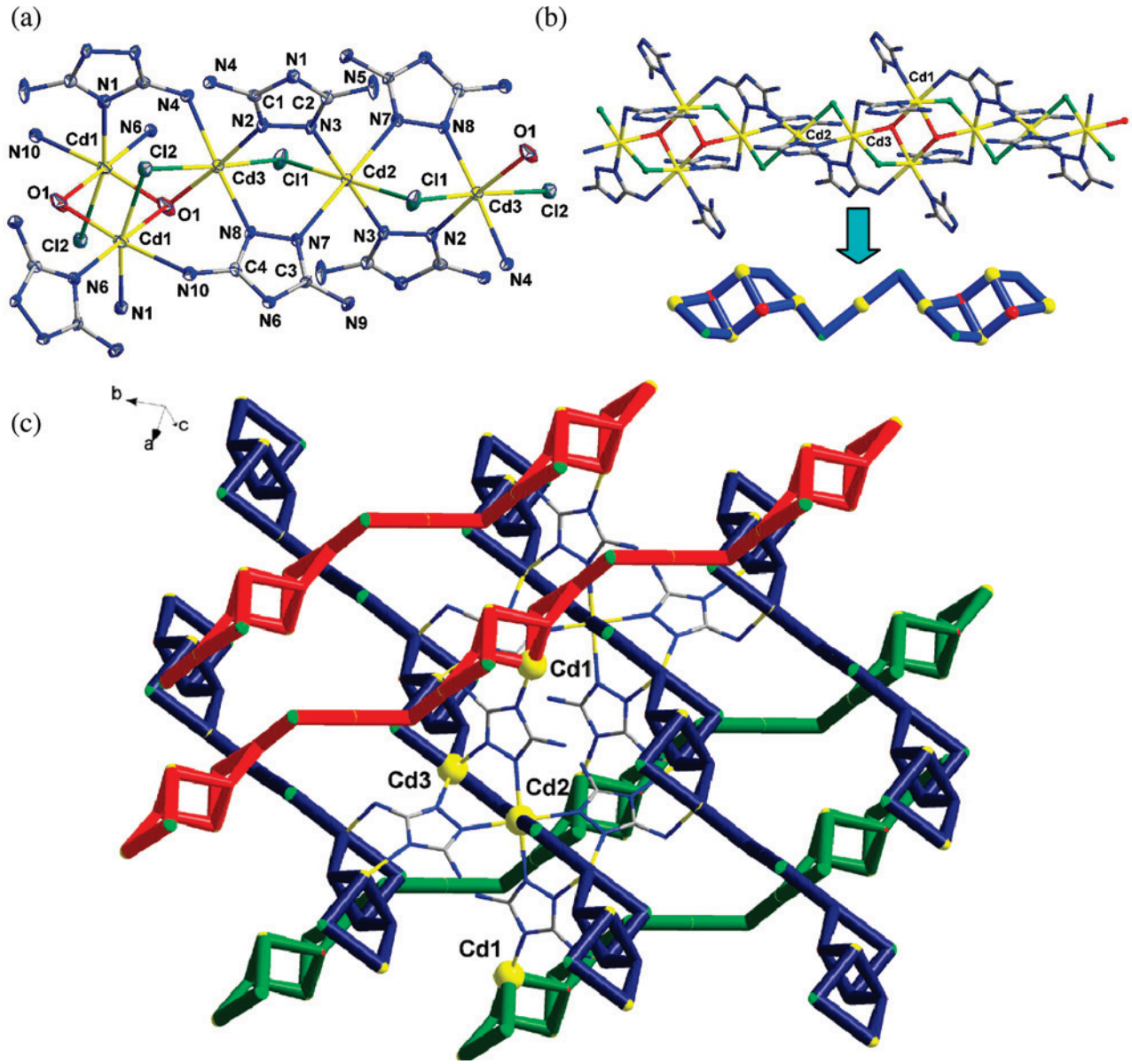

Figure 3. (a) ORTEP drawing of $[Cd_5(datrz)_4Cl_4(OH)_2]$ (**3**) showing the atom-labeling system and 50% thermal ellipsoids. H atoms have been omitted for clarity. (b) View of the chain substructure of **3** constructed by chair-like $\{Cd_4O_2Cl_2\}$ clusters with 2-connected $\{CdCl_2\}$ rods. (c) View of the 3D network of **3**.

and the methyl groups of the acetate ligands project outward from either face of the layer. It is noteworthy that there are two kinds of acetate groups in this structure: one adopting a η^2, μ_3 coordination mode, and the other only adopting a η^2 mode with their terminal methyl groups perpendicular to the *bc* plane. In addition, when observed along the *c*-axis, corrugated $\{Cd_3O_4\}_n$ ribbons with $\{Cd_2N_4\}$ heterocycles construct a one-dimensional (1D) channel, as shown in Figure 6c.

$EtCO_2^-$ Ions Controlled 2D Connectivity in [Cd(datrz)-(O_2CEt)] (7). The propionate phase [Cd(datrz)(O_2CEt)] (**7**) is a 2D structure (Figure 7b), which is constructed from a distorted square pyramidal $\{CdN_3O_2\}$ site ($\tau = 0.28$), defined by three guanazolate nitrogen donors and a propionate ligand, as shown in Figure 7a. The secondary building unit of **7** can be described as a binuclear $\{Cd_2(datrz)_2(O_2CEt)_2\}$ unit, with two cadmium centers bridged by two guanazolate ligands, affording a $\{Cd_2N_4\}$ heterocycle. In addition, each cadmium center also is bridged to the exocyclic N4 position, and thus, binuclear units are connected each other (through the bridging mode **D**) to propagate into a 2D layer structure, as shown in Figure 7b. When viewed along the [101] direction, the connectivity pattern of **7** can be described as a 2D quadrangular grid, as illustrated in Figure 7c.

In contrast, carboxylate groups of the propionate ligands in **7** only adopt a bidentate chelating mode, besides which, acetate carboxylate groups in **6** also serve as μ_2-bridged ligands. Consequently, the structure of **7** is prominently different from that of **6**. This difference can be partially attributed to the enhanced steric hindrance when the terminal methyl groups of the alkylcarboxylate ligands are replaced by the ethyl groups.

$^tBuCO_2^-$ Ions Controlled 2D Connectivity in [Cd-(Hdatrz)(O_2C^tBu)$_2$] (8). To enhance the steric hindrance further, the ethyl group of the alkylcarboxylate ligand is changed into the tertbutyl, obtaining a pivalate phase $[Cd(Hdatrz)(O_2C^tBu)_2]$ (**8**). As shown in Figure 8a, the

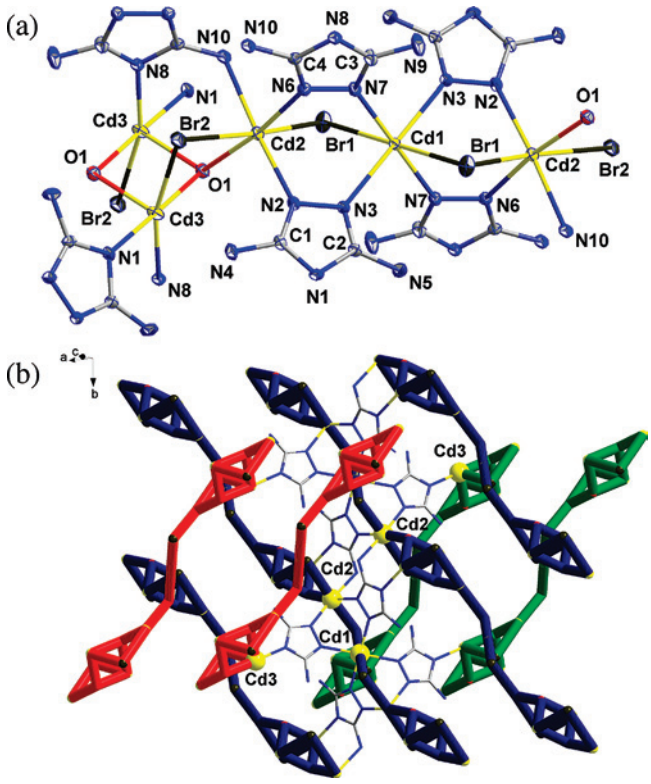

Figure 4. (a) ORTEP drawing of $[Cd_5(datrz)_4Br_4(OH)_2]$ (**4**) showing the atom-labeling system and 50% thermal ellipsoids. H atoms have been omitted for clarity. (b) View the 3D network of **4**.

coordination geometry of each cadmium site is a distorted octahedron, which is defined by four oxygen donors, a N1 (N2) nitrogen donor, and a N4 nitrogen donor. The structure of **8** can be considered as $\{Cd(Hdatrz)(O_2C^tBu)\}_n^{n+}$ zigzag chains running along the *b*-axis. Parallel chains are linked through μ_2-pivalate ligands producing a 2D corrugated layer structure, which propagates in the *bc* plane with tertbutyl groups projecting from either face of the layer (Figure 8b). In addition, there are two distinct pivalate ligands in **8**: one adopting a η^2 mode (which is also observed in **6** and **7**), and the other adopting a μ_2 mode through which eight-membered rings $\{Cd_2(CO_2)_2\}_n$ are formed between two chains (Figure 8b). Moreover, presumably because of the strong steric hindrance of the tertbutyl group of the pivalate ligand, the guanazole ligand in **8** only adopts the N1 (N2), N4-bridging mode (type **C** in Scheme 1) in a neutral form.

We note that three alkylcarboxylate anions $MeCO_2^-$, $EtCO_2^-$, and $^tBuCO_2^-$ controlled compounds **6**, **7**, and **8** all manifest a 2D structure, and in these complexes, there is no amino N nitrogen donor participated coordination. Thus, we believe that the alkylcarboxylate anions can induce low coordination numbers of the guanazole ligand and control the 2D connectivity of its complexes.

H_2Edta^{2-} Ions Controlled Discrete Cd(II)-Hdatrz Connectivity in $[Cd(Hdatrz)_2(H_2Edta)]$ (9). The EDTA phase $[Cd(Hdatrz)_2(H_2Edta)]$ (**9**) is the only zero-dimensional (0D) structure of this study. As shown in Figure 9a, the coordination polyhedron of each cadmium center is a distorted octahedral $\{CdN_4O_2\}$ site, with its equatorial plane occupied by two N1 (N2) nitrogen donors from guanazole ligands and

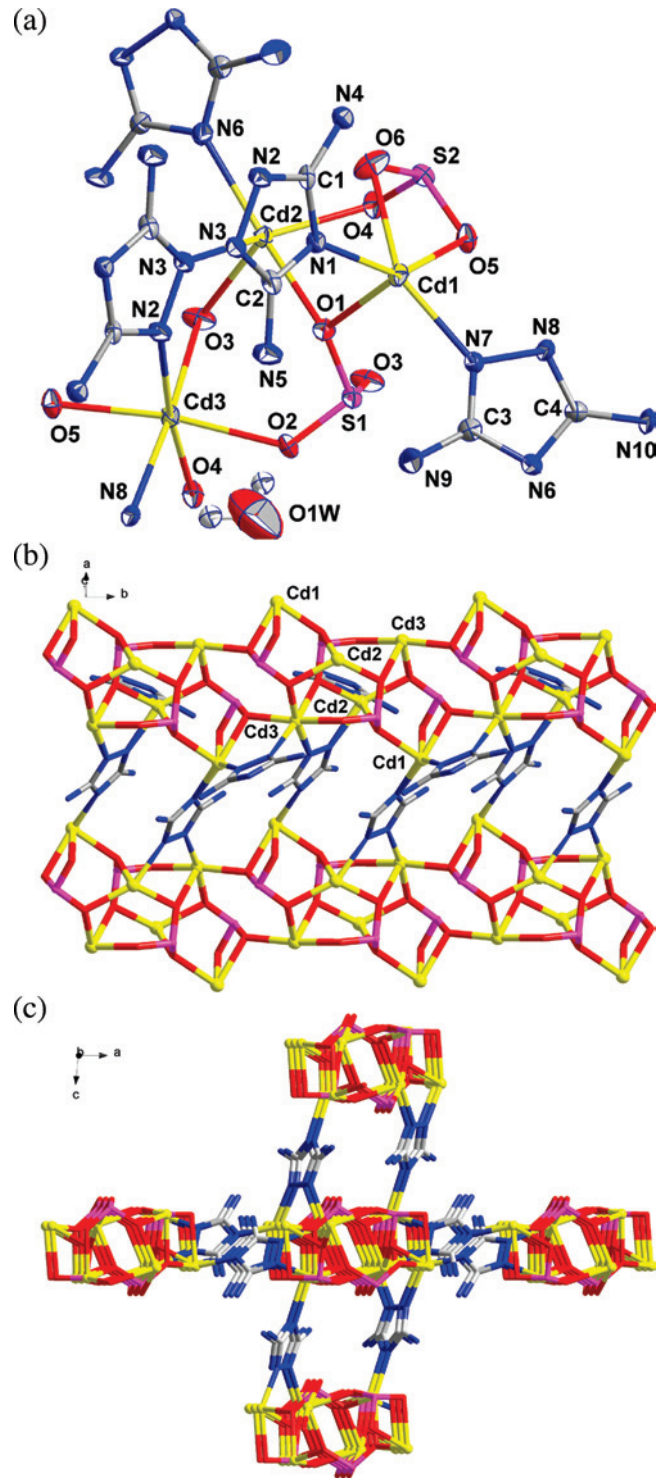

Figure 5. (a) ORTEP drawing of $[Cd_3(datrz)_2(SO_3)_2(H_2O)]$ (**5**) showing the atom-labeling system and 30% thermal ellipsoids. H atoms have been omitted for clarity. (b) View of the $\{Cd_3(SO_3)_2\}_n^{2n+}$ chains and the cage-like hexnuclear Cd−S−O clusters running parallel to the *b*-axis. (c) View of the 3D network of **5**.

two nitrogen donors from the H_2Edta^{2-} ligand, one of them bonding to the cadmium site in a bent mode out of the equatorial plane. Two axial oxygen atoms complete the cadmium coordination geometry with a small deviation.

In addition, hydrogen bonding and $\pi-\pi$ stacking interaction play an important role in forming this structure. As shown in Figure 9b, uncoordinated N4 and amino nitrogen

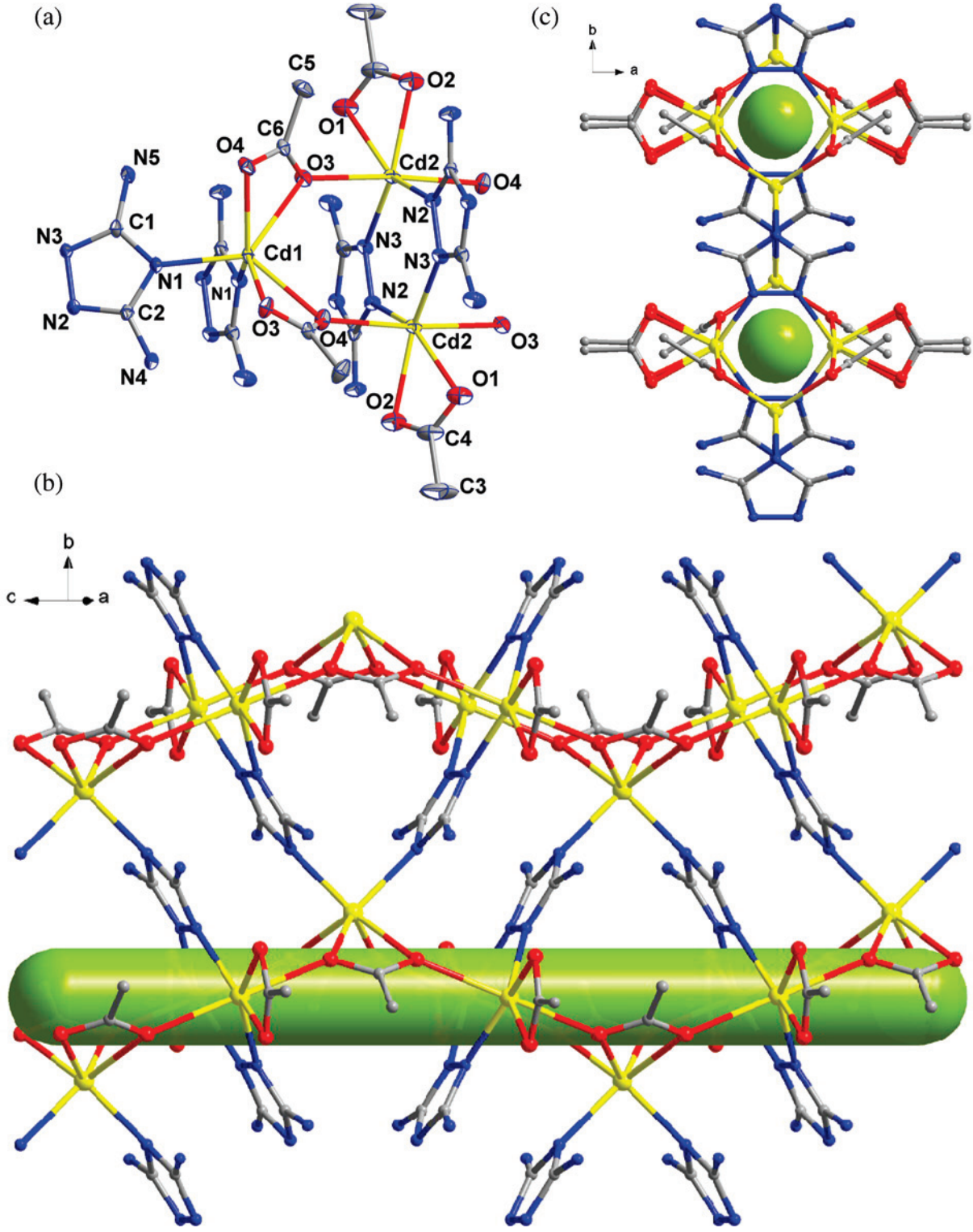

Figure 6. (a) ORTEP drawing of $[Cd_3(datrz)_2(O_2CMe)_4]$ (**6**) showing the atom-labeling system and 30% thermal ellipsoids. H atoms have been omitted for clarity. (b) View of the 2D layer structure and 1D channels of **6** constructed by corrugated $\{Cd_3O_4\}_n$ ribbons and guanazolate ligands. (c). View of the 1D channels of **6** observed along the *c*-axis direction.

sites are hydrogen-bonded to carboxylate oxygen sites of another molecular unit. Furthermore, guanazole five-membered heterocycles are aligned parallel to those of another molecular unit in an inverse offset face-to-face $\pi-\pi$ stacking mode. The plane-to-plane distance of this $\pi-\pi$ stacking is 3.226(Å), indicating a medium strong $\pi-\pi$ stacking interaction of this compound.

In summary, with effective control of inorganic or organic anions, the coordination diversity of the guanazole ligand in **1**−**9** manifests five bridging modes varying from bidentate

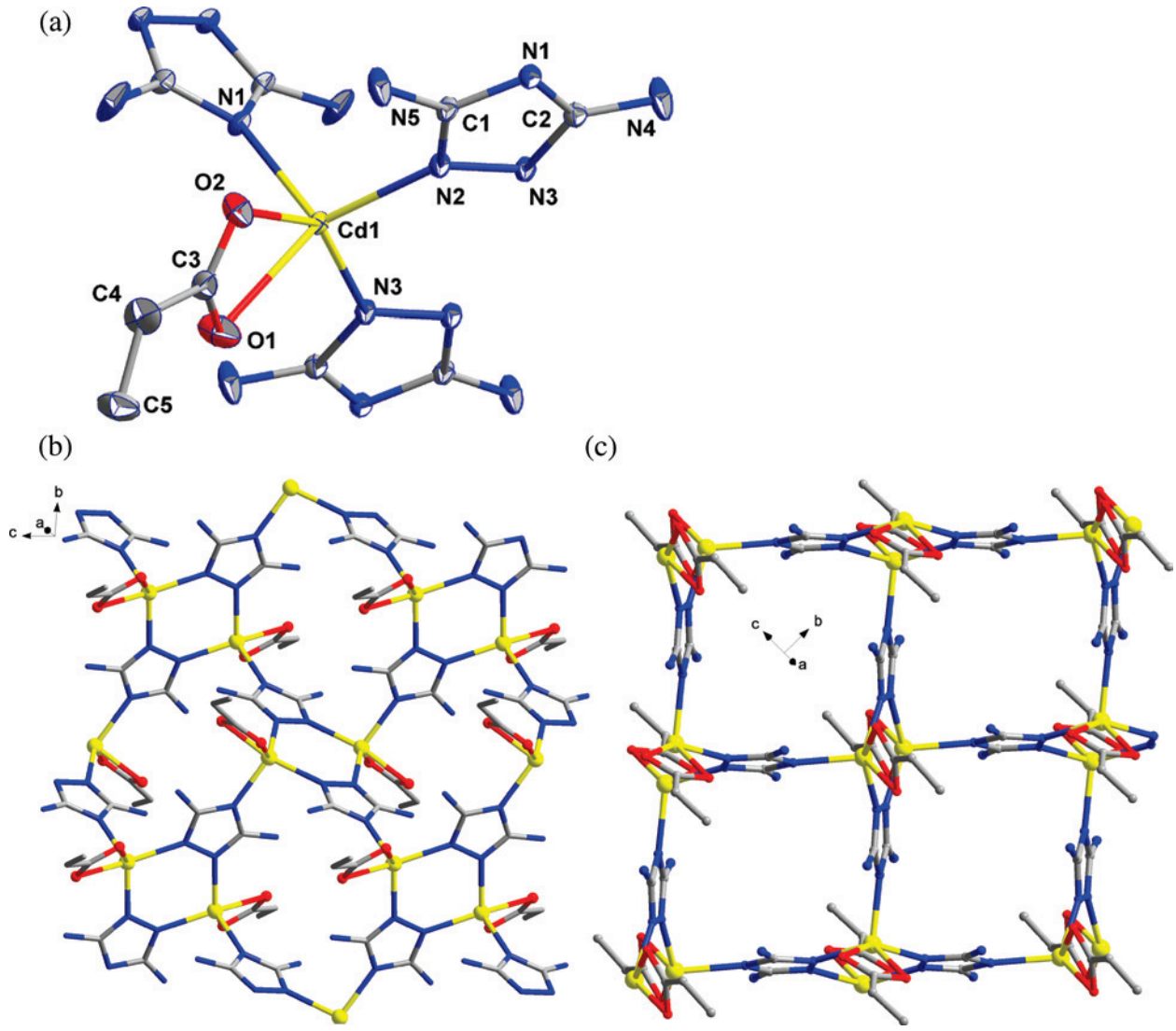

Figure 7. (a) ORTEP drawing of [Cd(datrz)(O_2CEt)] (**7**) showing the atom-labeling system and 30% thermal ellipsoids. H atoms have been omitted for clarity. (b) Representation of the connectivity pattern of **7**. (c) Two-dimensional quadrangular grid structure of **7** viewing along the [101] direction.

to quadridentate, as shown in Table 2. We conclude that the inorganic anions F^-, Cl^-, Br^-, and SO_3^{2-} can control a 3D connectivity, and particularly, halogen anions F^-, Cl^-, and Br^- can virtually induce high coordination numbers of the guanazole ligand, that is, the novel quadridentate bridging mode **F**, whereas low coordinantion numbers of the guanazole ligand can be induced by organic anions $MeCO_2^-$, $EtCO_2^-$, $^tBuCO_2^-$, and H_2Edta^{2-}, affording low dimensional structures with 2D or 0D connectivity. Neutral component H_2O can participate in the construction of a chiral 3D connectivity with the guanazole ligand adopting another unprecedented bridging mode **E**. In addition, the variability of coordination polyhedra is also well presented, such as square pyramid (for **4**, **5**, **7**), trigonal bipyramid (for **1**), trigonal prism (for **6**), and octahedron (for **1**−**6**, **8**, and **9**).

Nonlinear Optical Properties. Second-order nonlinear optical effects for the powder sample of **1** have been investigated by optical second-harmonic generation (SHG) at room temperature. The intensity of the green light (frequency-doubled output, $\lambda = 532$ nm) produced by the powder sample of **1** is about 0.2 times that produced by a potassium dihydrogen phosphate (KDP) powder, indicating that the compound **1** has a SHG effect that is weaker than that of KDP.[29] The weakness of the SHG effect for compound **1** may be presumably attributed to the influence of coordination water ligands in the crystal lattice.[28a,b]

Thermogravimetric Analysis (TGA). In this study the thermal stabilities of all compounds except **5** were analyzed on crystalline samples by TG/DTA from 40 to 900 °C at a rate of 10 °C min^{-1}, under an air atmosphere with a flowing rate of 20 mL min^{-1}; the thermal decomposition of compound **5** was especially studied by means of TGA-QMS, that is, a measurement of TG instruments on-line coupled with a quadrupole mass spectrometer, under 20 mL min^{-1} flowing

(29) The powder second-harmonic generation test was carried out on the sample by the Kurtz and Perry method. Second-harmonic generation intensity data were obtained by placing a powder sample in an intense fundamental beam from a Q-switched Nd:YAG laser of wavelength 1064 nm. The output ($\lambda = 532$ nm) was filtered first to remove the multiplier and was then displayed on an oscilloscope. This procedure was then repeated using a standard NLO material (microcrystalline KDP), and the ratio of the second-harmonic intensity outputs was calculated.

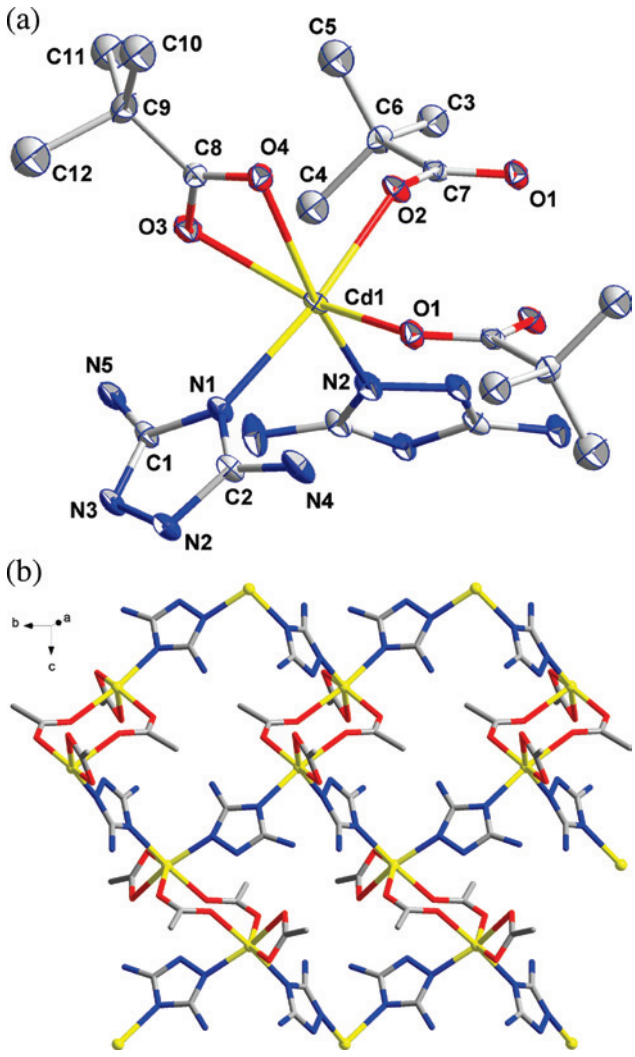

Figure 8. (a) ORTEP drawing of [Cd(Hdatrz)(O_2C^tBu)$_2$] (**8**) showing the atom-labeling system and 30% thermal ellipsoids. H atoms have been omitted for clarity. (b) View of the 2D corrugated layer structure of **8** (methyl groups in pivalates have been omitted for clarity).

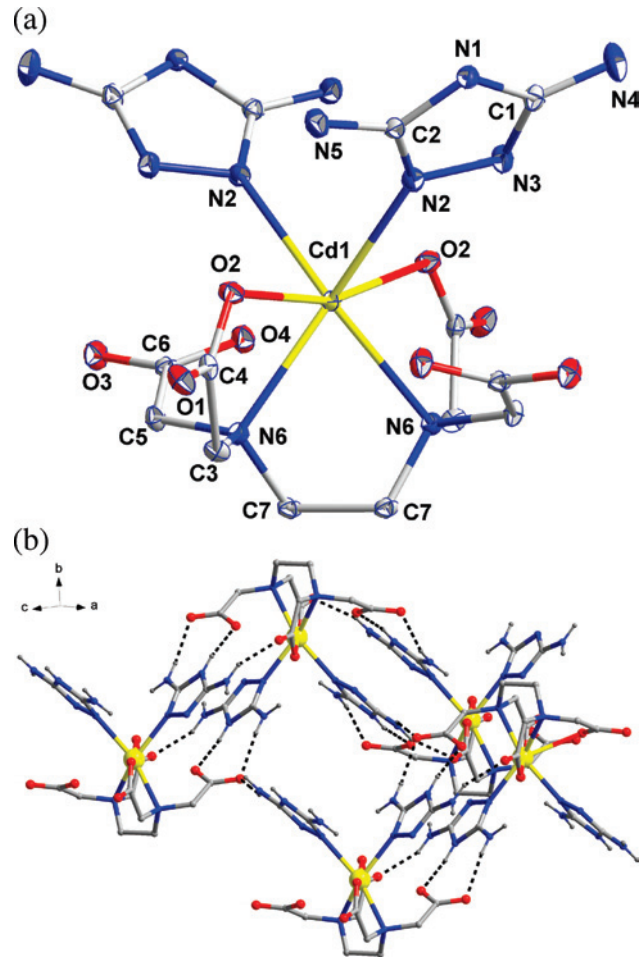

Figure 9. (a) ORTEP drawing of [Cd(Hdatrz)$_2$(H_2Edta)] (**9**) showing the atom-labeling system and 30% thermal ellipsoids. H atoms have been omitted for clarity. (b) View of the structure packing of **9** showing $\pi-\pi$ stacking interaction and hydrogen bonds (in dotted line).

nitrogen, at a rate of 10 °C min^{-1} from 40 to 1000 °C. The detailed temperatures and weight losses for **1**−**9** are given in the Supporting Information.

It is noteworthy that the TG curve of **2** (Figure 10a) is largely unchanged up to 450 °C, indicating that the framework of **2** is quite robust and thermally stable. The thermodiffraction profile of **2** (Figure 10b) shows that its structure framework is generally unchanged up to 550 °C, although **2** starts to lose organic components at 450 °C. This observation suggests that the partial loss of guanazolate ligands does not definitely lead to structural collapse of **2**, and its structural integrity can persist far beyond the partial decomposition temperature. In addition, complex **2** displays the highest thermal stability among all compounds of this study, and it is also higher than other reported fluoride phase Cd(II)-triazolate structures.[10] This remarkable property of **2** may be partially attributed to its quite strong Cd−F bond and quadridentate guanazolate ligand which possesses more coordination sites than tridentate triazolate ligand, and all these afford a more stable and dense framework, which needs more energy to break down.

Complex **1** and **3** also manifest high thermal stability with their TG curves unchanged from room temperature to 300 °C and 390 °C, respectively (Supporting Information, Figures S2a and S2b). In spite of being isomorphous to **3**, complex **4** is stable only up to 220°C (Supporting Information, Figure S2c). This may be partially attributed to their slight structure variation: because of a longer Cd−Br bond and less guanazolate coordination sites than that of **3**, complex **4** affords a looser 3D network with lower thermal stability. The TG curves of **6** and **7** are analogous, and this is related to their similar 2D structural skeletons. Both of them exhibit very little weight loss up to 350°C, manifesting a high thermal stability (Supporting Information, Figures S2d and S2e). Different from other complexes, complex **8** begins to lose weight at 175 °C (Supporting Information, Figure S2f), displaying the lowest thermal stability among all nine compounds. This may be caused by its guanazole ligand adopting low coordination numbers and its loose 2D structure, which is significantly expanded by the strong steric hindrance of the tertbutyl groups. The TG curve of **9** (Supporting Information, Figure S2g) illustrates that no weight loss is observed up to 300 °C, showing a high thermal stability of this material. Thermodiffraction profile of **9**

Table 2. Coordination Diversity of the Guanazole Ligand for **1**−**9**

complex	anion/ water	no. of datrz/Hdatrz	bridging modes and no. of datrz/Hdatrz	chelating no. of datrz/Hdatrz	structural dimension
1	H_2O	6	N1, N2 -bridging mode (**B**) × 3	bidentate	three
			N1, N2, N4-bridging mode (**D**) × 1	tridentate	
			N1, N2, amino N-bridging mode (**E**) × 2	quadridentate	
2	F^-	4	N1, N2, N4-bridging mode (**D**) × 2	tridentate	three
			N1, N2, N4, amino N-bridging mode (**F**) × 2	quadridentate	
3	Cl^-	4	N1, N2, N4, amino N-bridging mode (**F**)× 4	quadridentate	three
4	Br^-	4	N1, N2, N4-bridging mode (**D**) × 2	tridentate	three
			N1, N2, N4, amino N-bridging mode (**F**)× 2	quadridentate	
5	SO_3^{2-}	2	N1, N2, N4-bridging mode (**D**) × 2	tridentate	three
6	$MeCO_2^-$	2	N1, N2, N4-bridging mode (**D**) × 2	tridentate	two
7	$EtCO_2^-$	1	N1, N2, N4-bridging mode (**D**) × 1	tridentate	two
8	$^tBuCO_2^-$	1	N1/N2, N4-bridging mode (**C**) × 1	bidentate	two
9	H_2Edta^-	2	N1, N2-bridging mode (**B**) × 2	bidentate	zero

(Supporting Information, Figure S5) also suggests that its framework can persist up to 385 °C, which is quite above the initial decomposition temperature of **9**. As for complex **5**, TG coupled with QMS analysis reveal that its thermolysis procedure is miscellaneous and difficult to divide into distinct thermolysis steps as in other materials of this study. The

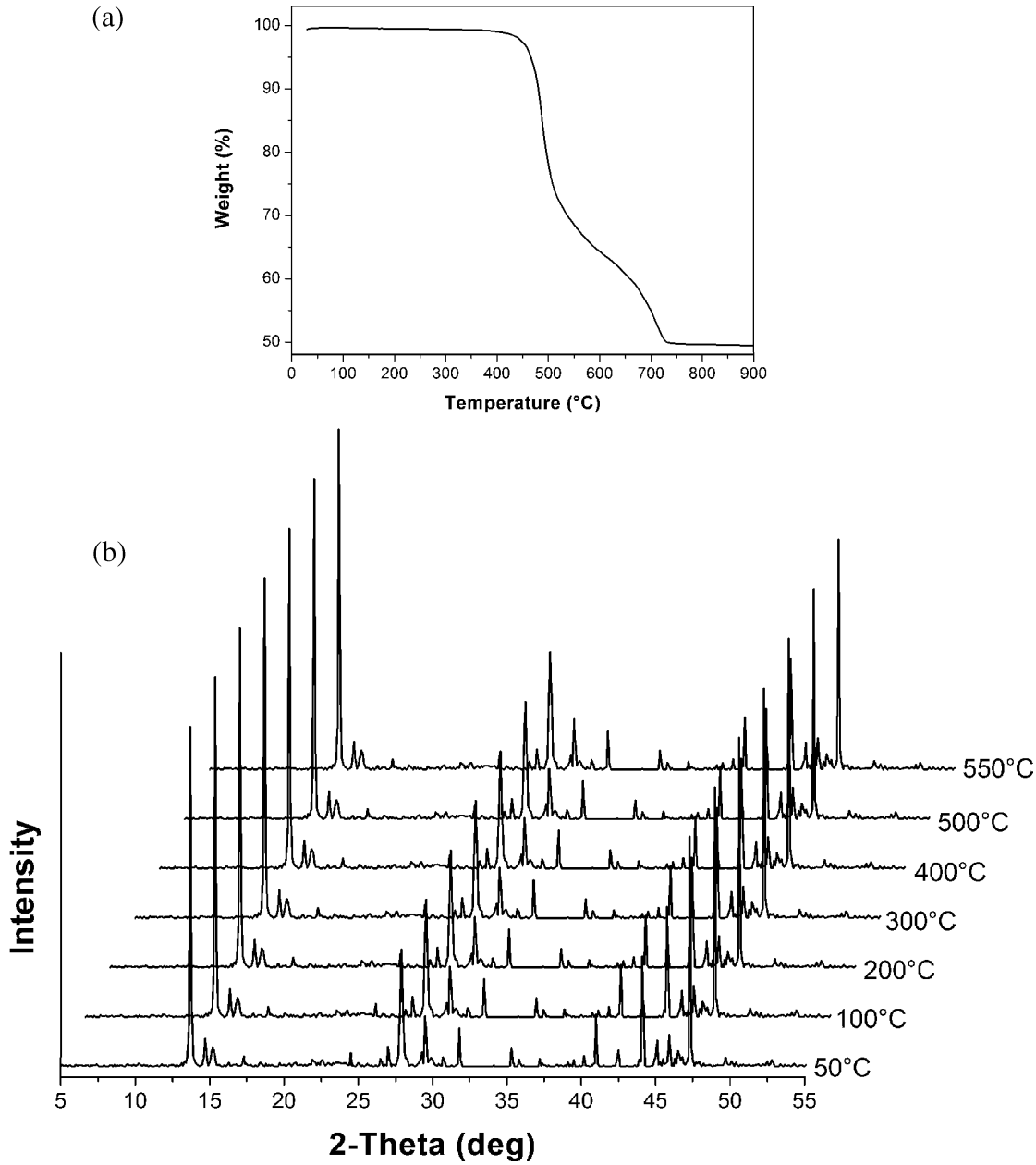

Figure 10. (a) TGA profile for **2**. (b) Thermodiffraction profile for **2** between 50 and 550°C.

detailed TG-QMS analysis of **5** is given in Supporting Information as well.

Photoluminescence Properties. Recently, luminescent Zn(II) and Cd(II) coordination complexes have been intensively investigated for their interesting fluorescence properties and potential applications as new luminescent materials,[30–33] for example, some zinc complexes have been reported to be used as organic light-emitting diodes (OLEDs).[34] Although the synthesis of the desired luminescent materials is still a challenge in this area, it is undoubted that appropriately incorporating conjugated organic ligands and anionic components into a coordination polymeric system is an efficient method to adjust luminescent properties of the materials, such as excitation/emission wavelength, intensity, lifetime, and so forth.

In this study, luminescence properties of all compounds have been explored at room temperature in the solid state because they are virtually insoluble in most common solvents such as acetone, methanol, chloroform, benzene, water, and so forth. Consequently, all complexes except **1** and **6** exhibit photoluminescence properties in the solid state. The absence of luminescence for **1** and **6** was unanticipated, and the explanation for this observation is not explicit and needing further investigation.

The free organic ligand guanazole displays such a weak luminescence that it can be negligible in the solid state. Therefore, for the sake of reference, its luminescence properties are explored in H_2O solution, obtaining a broad emission maximum at 435nm with excitation at 380 nm (Supporting Information, Figure S6). The main chromosphere of this ligand is the aromatic five-membered hetero ring and its photoluminescence is assigned as originating from $\pi-\pi^*$ transitions. Compared with 1,2,4-triazole, the maximum emission wavelength of guanazole is red-shifted, which is ascribed to that its electron-donating amino groups increase the conjugation degree of the parent aromatic ring.[35] Although the reason for the weakness of the photoluminescence in the solid state remains obscure, photoluminescence enhancement of the guanazole in H_2O solution may be partially associated with the hydrogen bonding interactions between amino groups and water molecules.

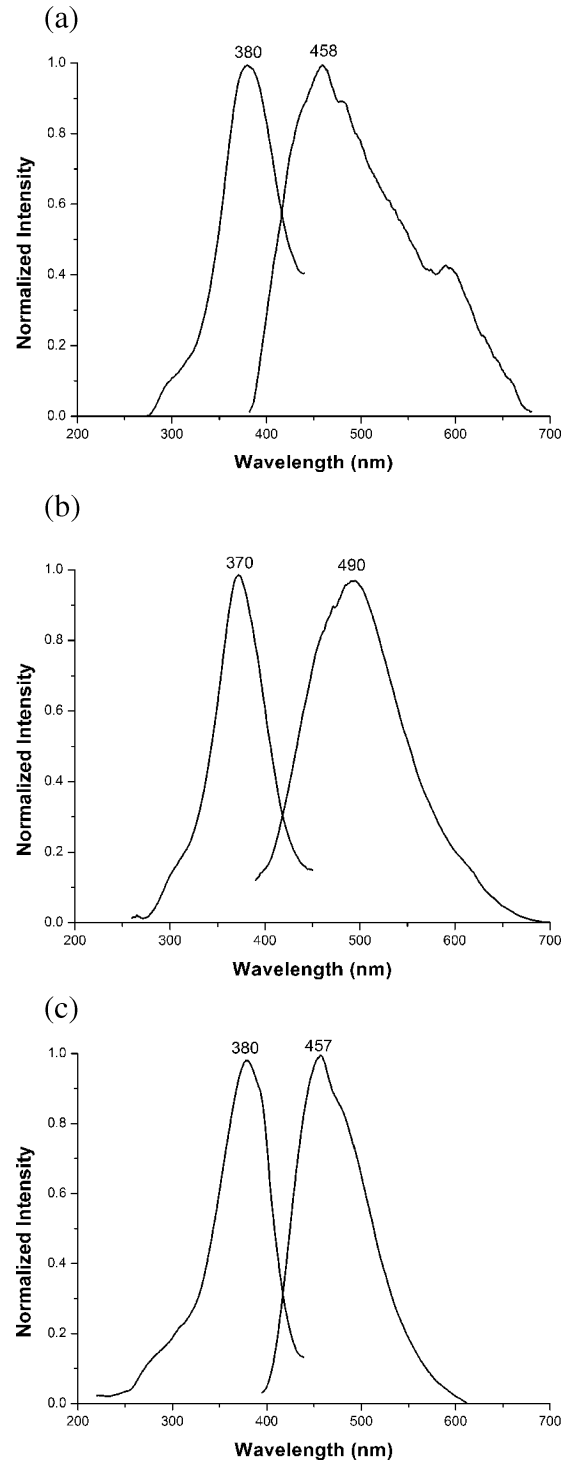

Figure 11. Excitation and emission spectra for **2** (a), **3** (b), and **4** (c) in the solid state at room temperature.

As shown in Figure 11a−c, compounds **2**−**4** exhibit blue fluorescent emission bands at 458 nm, 490 nm, and 457 nm upon excitation at 380 nm, 370 nm, 380 nm, respectively. In these compounds, the highest occupied molecular orbital (HOMO) is presumably associated with the π-bonding orbital from the guanazole ring, which is increasingly conjugated

(30) (a) Fabbrizzi, L.; Licchelli, M.; Rabaioli, G.; Taglietti, A. *Coord. Chem. Rev.* **2000**, *205*, 85. (b) Zheng, S. L.; Yang, J. H.; Yu, X. L.; Chen, X. M.; Wong, W. T. *Inorg. Chem.* **2004**, *43*, 830. (c) Fahrni, C. J.; O'Halloran, T. V. *J. Am. Chem. Soc.* **1999**, *121*, 11448. (d) Hirano, T.; Kikuchi, K.; Urano, Y.; Nagano, T. *J. Am. Chem. Soc.* **2002**, *124*, 6555.

(31) Ding, B.; Yi, L.; Wang, Y.; Cheng, P.; Liao, D. Z.; Yan, S. P.; Jiang, Z. H.; Song, H. B.; Wang, H. G. *Dalton Trans.* **2006**, 665.

(32) (a) Hao, N.; Shen, E. H.; Li, Y. G.; Wang, E. B.; Hu, C. W.; Xu, L. *Eur. J. Inorg. Chem.* **2004**, 4102. (b) Wu, B. L.; Yuan, D. Q.; Jiang, F. L.; Wang, R. H.; Han, L.; Zhou, Y. F.; Hong, M. C. *Eur. J. Inorg. Chem.* **2004**, 2695.

(33) (a) Zhang, J.; Xie, Y. R.; Ye, Q.; Xiong, R. G.; Xue, Z. L.; You, X. Z. *Eur. J. Inorg. Chem.* **2003**, 2572. (b) Dai, J. C.; Wu, X. T.; Fu, Z. Y.; Cui, C. P.; Hu, S. M.; Du, W. X.; Wu, L. M.; Zhang, H. H.; Sun, R. O. *Inorg. Chem.* **2002**, *41*, 1391. (c) Yuan, R. X.; Xiong, R. G.; Xie, Y. L.; You, X. Z.; Peng, S. M.; Lee, G. H. *Inorg. Chem. Commun.* **2001**, *4*, 384.

(34) (a) Cui, J.; Wang, A.; Edleman, N. L.; Ni, J.; Lee, P.; Armstrong, N. R.; Marks, T. J. *Adv. Mater.* **2001**, *13*, 1476. (b) Evans, R. C.; Douglas, P.; Winscom, C. J. *Coord. Chem. Rev* **2006**, *250*, 2093. (c) Berggren, K.; Chernokalskaya, E.; Steinberg, T. H.; Kemper, C.; Lopez, M. F.; Diwu, Z.; Haugland, R. P.; Patton, W. F. *Electrophoresis* **2000**, *21*, 2509. (d) Sapochak, L. S.; Benincasa, F. E.; Schofield, R. S.; Baker, J. L.; Riccio, K. K. C.; Fogarty, D.; Kohlmann, H.; Ferris, K. F.; Burrows, P. E. *J. Am. Chem. Soc.* **2002**, *124*, 6119.

(35) Valeur, B. *Molecular Fluorescence: Principles and Applications*; Wiley-VCH: Weinheim, 2001.

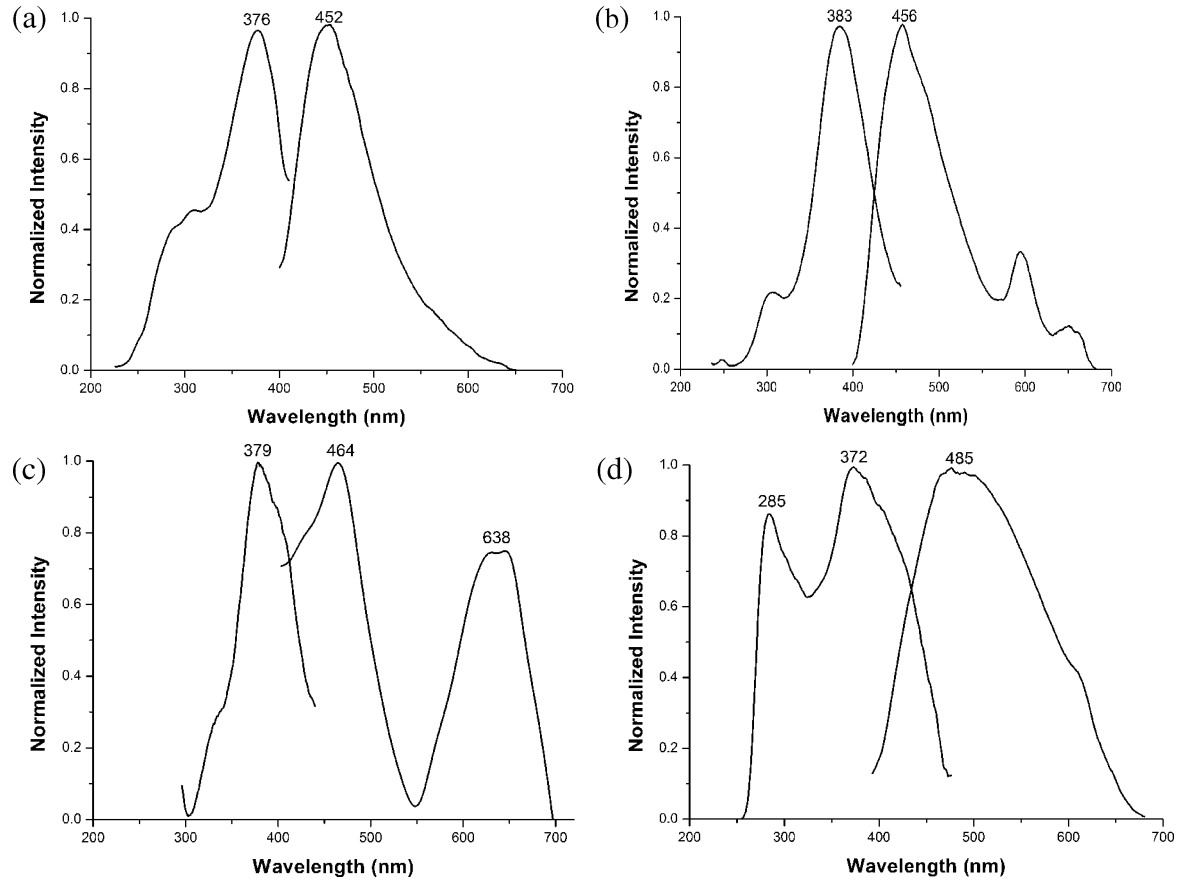

Figure 12. Excitation and emission spectra for **5** (a), **7** (b), **8** (c), and **9** (d) in the solid state at room temperature.

by the electron-donating amino groups, and the lowest unoccupied molecular orbital (LUMO) may be dominated by the ligand π^* character rather than the Cd−X (X = F, Cl, Br) σ^* orbital because the heteroatoms in the aromatic ligand can effectively decrease the π and π^* orbital energies.[36] Thus, the HOMO and LUMO, as well as the orbitals with energies close to them, may lack a significant contribution from the metal atoms. Therefore, luminescence behaviors of **2**−**4** may be assigned as the intraligand $\pi-\pi^*$ transitions. This assignment is also supported by the density functional theory (DFT) calculation results of the similar triazolate complex [Zn(trz)Cl] reported by Zubieta et al.[10] It is noteworthy that compound **3** exhibits a red shift of 30 nm for its emission band in contrast to **2**, which may be ascribed to the reduction in the HOMO−LUMO gap of **3** caused by structural change. Though compound **4** is isomorphous with **3**, their fluorescent bands are obviously different. This is because two of the five cadmium centers in **4** are five-coordinated, and this coordination mode has more electron-pulling effects on the guanazolate ligand,[36] making a larger HOMO−LUMO energy gap than **3**, in which all cadmium centers are six-coordinated. Consequently, **4** manifests a blue shift of 30 nm from the emission of **3**.

Similar to **2**−**4**, compounds **5** and **7** display blue fluorescent emission bands at 452 nm and 456 nm, with the excitation at 376 nm and 383 nm, respectively (Figure 12a,b). Their luminescence behaviors may be also assigned as the intraligand $\pi-\pi^*$ transitions. It is revealed that neither sulfite nor propionate anions may significantly influence the photoluminescence properties of Cd(II)-guanazole complexes. As for compound **8**, besides the characteristic blue emission at 464 nm (λ_{ex} = 379 nm) originating from the intraligand $\pi-\pi^*$ transitions, an unusual orange emission at 638 nm is observed as well (Figure 12c). The latter emission has never been reported in polymeric Zn(II) or Cd(II) complexes, and it may possibly come from the pivalate ligand because a similar emission can be observed from the free pivalic acid ligand (λ_{em} = 620 nm with excitation at 274 nm in the solid state, Supporting Information, Figure S7).

For compound **9**, a broad blue to green emission is exhibited with the maximum at 485 nm (λ_{ex} = 372 nm), which may be assigned as the intraligand $\pi-\pi^*$ transitions similar to other compounds of this study. However, the excitation scan at this emission wavelength gives another peak at 285 nm besides the peak at 372 nm (Figure 12d). This observation is unanticipated and might be correlated with the absorption characteristics of the H_2EDTA ligand at this wavelength.[37,38] Moreover, the emission red shift of **9** in contrast to other compounds is presumably attributed to a reduction of the HOMO−LUMO gap, which may be caused by the amine lone-pair electrons of the H_2EDTA ligand increasing the HOMO energy. In addition, the mixed-

(36) Zheng, S. L.; Chen, X. M. *Aust. J. Chem.* **2004**, *57*, 703.

(37) Laamanen, P. L.; Mali, A.; Matilainen, R. *Anal. Bioanal. Chem.* **2005**, *381*, 1264.

(38) Inoue, M. B.; Machi, L.; Munoz, I. C.; Rojas-Rivas, S.; Inoue, M.; Fernando, Q. *Inorg. Chim. Acta* **2001**, *324*, 73.

ligand system (H_2EDTA and guanazole) may cause multiple charge-transfers within close transition energies, which might ultimately result in a broad emission band.[39]

It is known that EDTA type fluorescent molecular sensors exhibit high selectivity for some alkaline earth metal ions through efficiently chelating interaction,[35] whereas there is no report about the solid photoluminescence of the EDTA chelated Cd(II) complexes. Among all materials of this study, compound **9** shows some remarkable properties: the strongest fluorescent intensity, the largest single crystal size (up to 5mm, Supporting Information, Figure S8), the highest yield (>95%), good crystal quality (Supporting Information, Figure S8), high thermal stability, as well as the moderate hydrothermal synthesis condition. All these properties enable **9** to be an excellently promising candidate for advanced blue-light-emitting luminescence materials.

Conclusions

In this study, a new hybrid family of nine Cd(II)-guanazole complexes **1**−**9** has been synthesized by exploiting hydrothermal methods, and all materials except **1** comprise various inorganic or organic charge-balancing anions, affording a general scheme of Cd(II)/datrz(or Hdatrz)/X, X = H_2O, F^-, Cl^-, Br^-, SO_3^{2-}, $MeCO_2^-$, $EtCO_2^-$, $^tBuCO_2^-$, and H_2Edta^-. With effective control of these anions, the coordination diversity of the guanazole ligand in **1**−**9** manifests an unprecedented enrichment with five bridging modes (type **B**−**F**) varying from bidentate to quadridentate, two of which are first reported (type **E** and **F**). Compound **1** is the first chiral compound constructed from the guanazole ligand which adopts a novel N1, N2, amino N-bridging mode (type **E**), and it also provides a promising approach to synthesize new chiral complexes with intriguing properties. Three halide phase compounds **2**−**4** are all 3D, with their guanazole ligands possessing another novel quadridentate bridging mode (type **F**). The di-negatively charged sulfite phase **5** also displays a 3D network with unprecedented cage-like hexnuclear cadmium clusters, whereas low dimensional structures have been found for alkylcarboxylate anions $MeCO_2^-$, $EtCO_2^-$, and $^tBuCO_2^-$ controlled **6**, **7**, and **8** (2D) and for H_2Edta^{2-} controlled **9** (zero- dimensional), and their guanazole ligands manifest low coordination numbers as well. In compounds **6**−**8**, there no amino N nitrogen donor participated coordination. Furthermore, the variability of the coordination polyhedra is also well presented, such as square pyramid (for **4**, **5**, **7**), trigonal bipyramid (for **1**), trigonal prism (for **6**), and octahedron (for all except **7**). Therefore, a rich structural chemistry of the Cd(II)-guanazole hybrid family has been accomplished through control of the anions, and this will contribute to the search and the design of new molecular structures.

From this study, we realize that a larger number of complexes with interesting structures can be successfully synthesized by modifying reaction variables, like temperature, pH value, stoichiometric ratio, starting reactants, and so forth. When the pH value was adjusted above 8.0, all obtained products were chiral compound **1**, regardless of any anionic component, and $Cd(NO_3)_2 \cdot 4H_2O$ was chosen as the appropriate starting material which could afford Cd^{2+} ions exclusively.

In addition, structure related physical properties of these complexes are also accentuated because of their potential applications as advanced functional materials. The chiral compound **1** exhibits the second-order nonlinear optical properties at room temperature. Except for **1** and **6**, all compounds exhibit photoluminescence of blue fluorescent emissions in the solid state at ambient temperature, which may be assigned to the intraligand $\pi-\pi^*$ transitions. Some structure induced red or blue shifts in emission bands are discussed, as well as the multiple excitation/emission bands in mixed-ligand systems. Most compounds of this study show a high thermal stability, which is further demonstrated by that partial loss of guanazole ligands does not result in structural collapse, and all nine compounds are almost insoluble in most common solvents. All these properties enable the title complexes to be used as thermally stable, solvent-resistant, and blue-light-emitting luminescent materials. Of all materials in this study, compound **9** gives prominence to be the best candidate for practical utility.

Acknowledgment. This work was supported by the State Key Basic Research and Development Plan of China (2007CB815302), the Chinese Academy of Sciences (KJCX2-YW-M05), the NSF (E0620005) of Fujian Province, the Major Special Foundation of Fujian Province (2005HZ1027, 2005HZ01-1), and the Fund of Fujian Key Laboratory of Nanomaterials (2006L2005).

Supporting Information Available: Crystallographic data in CIF format, X-ray powder diffraction patterns for **1**−**9**, detailed thermogravimetric analysis for **1**−**9**, thermodiffraction pattern for **5** and **9**, excitation and emission spectra for guanazole, emission band for pivalic acid, photograph of crystals of **9**, and selected bond lengths and angles for **1**−**9** (PDF). This material is available free of charge via the Internet at http://pubs.acs.org.

IC8001042

(39) Shi, X.; Zhu, G. S.; Fang, Q. R.; Wu, G.; Tian, G.; Wang, R. W.; Zhang, D. L.; Xue, M.; Qiu, S. L. *Eur. J. Inorg. Chem.* **2004**, 185.